Physics – Uspekhi **38** (3) 253 – 271 (1995)

©1995 Jointly Uspekhi Fizicheskikh Nauk and Turpion Ltd

REVIEWS OF TOPICAL PROBLEMS

PACS numbers: 36.40.−c; 47.53.+n; 61.43.Hv

The generation of fractal structures in gaseous phase

E F Mikhailov, S S Vlasenko

Contents

Abstract. Peculiarities of fractal cluster growth in the gaseous phase are analysed. The effect of thermal and ionised particles on the structure of forming aggregates is considered. Special attention is paid to the analysis of experimental methods of generating fractal clusters. The role of charges and electric fields in the growth of fractal structures is demonstrated. The influence of the geometry of fractal objects on their aerodynamic, sorption, and kinetic characteristics is analysed on the basis of experimental data.

1. Introduction

Application of the fractal geometry concept to physics dates from the 1970s when fundamental works of Mandelbrot [1] were first published. Since that time, the theory of fractal systems has been successfully employed to analyse the structure and the properties of objects formed in the course of nonequilibrium processes. Such objects include fractal clusters, i.e. structures resulting from coagulation of solid particles which move along certain trajectories.

The clusters are normally supposed to consist of nanometer particles although there is only one formal limitation imposed on the size of their constituent elements, which is that they must be considerably smaller than the agglomerate. From this standpoint, clusters of galaxies in the Universe are also considered to be fractal clusters [2].

A fractal cluster is a convenient object to use in constructing numerical models intended to simulate the effect of growth conditions on the aggregate structure. Current knowledge of these objects largely stems from the use of computer models. Fractal growth models have been extensively discussed in the literature and reviewed in a few recent publications [3, 4]. At the same time, certain authors appear to be increasingly interested in exploring the properties of fractal aggregates [5].

This interest can be attributed to at least two causes. In the first place, fractal clusters have been found to occur frequently in nature. For example, it has been shown that certain species of atmospheric aerosols (e.g. smoke particles) and some types of stratospheric aerosols are in fact fractals. This accounts for the great attention paid to studying their optical [6, 7, 8, 9] and transport [10, 11] properties which are supposed to be responsible for the degree of their involvement in atmospheric processes.

Secondly, the fractal cluster is the principal structural element in a number of macroscopic systems known to emerge from physicochemical processes and events that resemble fractal growth phenomena [12]. Of late, many studies dedicated to this class of objects have focused upon aerogels, i.e. macroscopic systems of very low density with well-developed porous structure and large specific surface.

In terms of properties, aerogels may actually be regarded as a new physical state of matter intermediate between gaseous and condensed states [13]. Such structures have been reported to possess a specific combination of physicochemical properties [14] which look very promising in the context of their technological application.

E F Mikhailov, S S Vlasenko Physics Research Institute, St. Petersburg State University, ul.Ulyanovskaya 1, 198904 Petrodvorets, St. Petersburg
Tel. (7-812) 428-45 72
Fax (7-812) 428-72 40
E-mail: mikh@acro.phys.pu.ru

Received 30 June 1994; revised 26 October 1994
Uspekhi Fizicheskikh Nauk **165** (3) 263–283 (1995)
Translated by Yu V Morozov; edited by H Milligan

Unfortunately, our present understanding of the structure and properties of fractal aggregations is largely based on the analysis of theoretical models and poorly supported by experimental findings. The main reason for this is the notorious technical difficulty with these objects of experimentation, which is both challenging and laborious.

A major methodological problem which needs to be solved to facilitate experimental studies is caused by the lack of an approach to the synthesis of aggregates with the broad spectrum of structural characteristics necessary to obtain structure-related information about physical and chemical properties of fractal clusters. Equally important is a reliable system of diagnostic tools to characterise structural parameters.

The former problem can only be solved with deeper insight into the processes responsible for the development of fractal aggregate structure. Computer models of cluster growth used to simulate extreme physical situations provide only a rough approximation to the solution of the problem.

The main reason for the disparity between numerical models and real aggregation experiments is that growth models a priori fix the aggregation patterns (cluster – cluster or cluster – particle), motion of clusters and particles (rectilinear or Brownian), and probability of coagulation during their interaction, whereas in cluster generation experiments these growth parameters are subject to continuous variation.

In the course of evolution of a dispersed gas system, the initial interaction of the cluster – particle type associated with rectilinear motion (kinetic regime) turns at a later stage into an interaction between clusters with Brownian motion. At intermediate stages, the particles appear to be involved in mixed interaction, with the contribution of either mechanism being variable in space, owing to density fluctuations.

The pattern becomes even more complicated under the influence of various processes on the surface of interacting particles, especially when they carry a charge. Specifically, charge redistribution between the particles automatically affects coagulation. The natural result of the diverse processes taking place in a real physical milieu is a marked difference between the structural parameters of aggregates formed under these conditions and those obtained in numerical simulations.

The above facts to a certain extent determined the choice of research strategy with respect to the properties of fractal aggregates. Earlier studies attempted to elucidate how conditions in which aggregates were generated influenced their structure. Analysis of experimental findings indicates that the structure of an aggregate formed in the gaseous phase is largely dependent on the parameters of the initial stage of this process. With this in mind, it is convenient to distinguish between high-temperature and low-temperature techniques for preparing fractal aggregates.

As a rule, high-temperature methods are used to vaporise refractory metals. These techniques include wire explosion [15], laser evaporation [16, 17], and arc discharge [18, 19]. Lower-temperature techniques provide for milder sublimation of starting materials with melting temperature below 1000 K [20].

An essential feature of high-temperature techniques is the formation of dense plasma near the surface with a temperature of several thousands of degrees and pressure in the range of few to tens of atmospheres. Relaxation of such a system is accompanied by the very fast (within 10^{-2} s) production of fractal clusters because of the initially high primary particle number density [13].

All attempts to significantly increase characteristic times of individual stages of the process and make them directly observable have been in vain because the plasma system remains stable in a rather narrow range of ambient parameters.

This explains why the mechanism of cluster formation in an ionised medium has to be understood from the structure of the aggregates produced and also from theoretical considerations, including those which ensue from the use of numerical models. Analysis of fractal cluster growth in a weakly ionised medium is presented in Section 2 of the present review.

Substances with low melting temperature appear to provide a better opportunity for the detailed examination of selected growth stages of fractal clusters and also an advantage in terms of the experimental technique. High vapour pressure for such substances is attainable at moderate temperature when ionisation of the medium is low and unlikely to have marked effect on the development of the system.

In this situation, it is easy to select conditions under which characteristic times of individual aggregation stages would increase to such an extent as to make it possible to simplify the experimental techniques considerably and design studies without sophisticated equipment. Methods for generation and structural analysis of fractal clusters are described in Section 3 which also contains some experimental data on fractal growth dynamics.

Section 4 is devoted to the experimental studies on aggregate structure modification in an electric field. Moreover, this section examines the relationship between the structure of aggregates and their aerodynamic and sorption characteristics.

2. Formation of aggregates upon relaxation of aerosol plasma

In a real aggregation experiment, the structure of fractal clusters is markedly dependent on the conditions in which they are obtained. This dependence is apparent at all stages of the system evolution, from vapour condensation into primary kernels to the formation of large aggregates.

At an early growth stage, the structure of the aggregates produced is greatly influenced by the degree of ionisation of the medium and also by the size, shape, and density of the number of primary kernels. If cluster assemblage occurs at relatively low temperature, the dispersed system becomes responsive to external fields. Specifically, electric fields have a marked effect on the structure of fractal clusters.

Since field modulation is the simplest and most readily available method of structural modification of growing clusters, it seems appropriate to examine factors which contribute to their directional growth under the influence of an electric field and to describe processes responsible for the formation of fractal clusters during the evolution of vapours as they cool down.

2.1 Condensation process in weakly ionised plasma

It has already been mentioned that fractal clusters are normally obtained in gaseous phase by heating the starting materials to high temperature. It is essential that the primary vapour–gas medium is a high-temperature mixture composed of atoms (or molecules) and charged particles, regardless of the method of supplying energy to the system (electric current, chemical reaction of combustion).

Evolution of such a system depends on the presence of ions which are the main sites of condensation of atoms and formation of growing microparticles initiated by fast cooling. The density of ions is therefore crucial for the size of primary kernels and serves as a rate-limiting factor. It is important to examine changes in the ionisation state of the system at different stages of cooling.

To begin with, the system is in ionisation equilibrium which is described by the Saha equation for density of charged particles. The time needed for the ionisation equilibrium to be reached increases as plasma cools down. This may account for disequilibration of the system under certain conditions. Therefore, cooling results in a higher density of charged particles compared with equilibrium density.

In the case in question, electron (or ion) density N_e is defined by the balance equation [21]:

$$\frac{dN_e}{dt} = k_r N_e (N_S^2 - N_e^2) \ , \tag{1}$$

where N_S is the equilibrium electron density described by the Saha equation and k_r is the rate constant for triple recombination of electrons and ions.

Eqn (1) suggests that electrons and ions are formed during stepwise ionisation of atoms, and that they are removed by triple recombination. The equilibrium electron density N_S changes with time t, as does the plasma temperature. It may be defined by the equation $N_S(t) = N_S(0)\exp(-\gamma t/2)$.

If $N_S^2 \sim \exp(-I/k_B T)$ (where I is the atomic ionisation potential, T is plasma temperature, and k_B is the Boltzmann constant), then

$$\gamma = \frac{I}{k_B T^2}\left|\frac{dT}{dt}\right| \ . \tag{2}$$

This means that Eqn (1) may be written as

$$\frac{dN_e}{dt} = k_r N_e \left[N_S^2(0)\exp(-\gamma t) - N_e^2\right] \ . \tag{3}$$

The asymptotic solution of this equation in the region where equilibrium is drastically disturbed has the form

$$N_e = \left(2\int_{t_0}^{t} k_r \, dt\right)^{-1/2} \ . \tag{4}$$

(if the process of ionisation is disregarded).

Now, we have to determine parameter t_0. This requires the asymptotic solution of Eqn (3) to be found on the assumption that the recombination rate constant k_r is independent of time. This assumption is valid because $N_S(T)$-dependence is stronger than $k_r(T)$.

The asymptotic solution of Eqn (3) may be presented in the following form:

$$\frac{1}{N_e^2(t)} = \frac{2k_r}{\gamma}\left[\gamma t - \ln\frac{2k_r N_S^2(0)}{\gamma} - C\right] \ , \tag{5}$$

where C is Euler's constant. Evidently, this solution does not depend on the choice of initial time t_0.

Comparison of Eqn (5) with expression (4) in the form of $N_e^{-2} = 2k_r(t - t_0)$ allows parameter t_0 to be found:

$$\gamma t_0 = C + \ln\frac{2k_r N_S^2(0)}{\gamma} \ . \tag{6}$$

This relation in fact indicates that the recombination time and the time of plasma density change in the region of disturbed ionisation equilibrium are similar.

Let us now derive the asymptotic expression for electron (ion) density. In the parameter range in question, $k_r \sim T^{-9/2}$ [22]. After a series of calculations, this dependence can be presented as [23]

$$k_r/\text{cm}^3\ \text{s}^{-1} = 6.4 \times 10^{-22}\left(\frac{1000}{T/\text{K}}\right)^{9/2} \ . \tag{7}$$

If plasma is assumed to dilate adiabatically, then $(T \propto 1/R)$

$$\frac{dT}{dt} \propto \frac{dT}{dR} T^{1/2} \propto T^{5/2} \ ,$$

where R is the distance from the evaporation spot. In this case, Eqn (4) takes the form of

$$\frac{1}{N_e^2} = 2\int_{t_0}^{t} k_r \frac{dT}{dT/dt} = \frac{T k_r(T)}{3\, dT/dt}\left[1 - \left(\frac{T}{T_i}\right)^6\right] \ , \tag{8}$$

where T is plasma temperature at a given point and $T_i = T(t_0)$ is temperature at the lower boundary of the region of marked ionisation disequilibrium (where $N_S \ll N_e$) which, according to Eqn (5), fulfils equation

$$k_r(T_i) N_S^2(T_i) = \frac{e^{-c}}{2}\frac{I}{k_B T_i^2}\left(\frac{dT}{dt}\right)_{T_i} \ . \tag{9}$$

Table 1 presents calculated parameters which characterise the ionisation state of copper plasma formed during laser evaporation of surface atoms. It is estimated that about 30 % of the laser radiation power is expended to produce copper vapour. The coefficient of accommodation of copper atoms to clusters (on collision with their surfaces) is 0.2.

Table 1. Characteristics of laser-induced copper plasma.

	Radiation flux/W cm^{-2}		
	10^7	3×10^6	10^6
T_0/K	7340	5440	4440
N_0/cm^{-3}	1.1×10^{20}	4.1×10^{19}	1.6×10^{19}
T_1/K	4910	3640	2950
N_1/cm^{-3}	2.8×10^{19}	1.0×10^{19}	4.0×10^{18}
p_1/atm	19	5.0	1.6
T_c/K	3270	2720	2360
N_c/cm^{-3}	1.5×10^{19}	6.4×10^{18}	2.9×10^{18}
T_i/K	5300	5000	4800
N_e/cm^{-3}	2.1×10^{14}	1.4×10^{14}	1.0×10^{14}
N_e/N_S^{-1}	62	1200	17 000
r_0/nm	17	12	7.3

The calculations are made for the case in which buffer gas pressure is much lower than the pressure of the substance being evaporated, and the plasma beam propagates at acoustic speed. In this case, the temperature of a single-atom gas in beam T_1 is related to the surface temperature T_0 by $T_1 = 0.67\,T_0$ while $N_1 = 0.25\,N_0$ holds for the relationship between atom density in beam N_1 and saturated vapour density N_0 [21].

The vapour density at temperature T_1 is somewhat lower than the saturated vapour density. This accounts for condensation starting at some distance from the irradiated surface where the beam dilates and the temperature drops accordingly to T_c. Density N_1 at this temperature is close to the saturated vapour density N_c [24].

Table 1 lists values of T_i , electron (ion) density N_e on the saturation line, and the ratio N_e/N_S (where N_S is equilibrium electron density). This ratio characterises the degree to which ionisation equilibrium is distributed on the saturation line.

The next stage of evolution of a gas–plasma system during cooling is condensation. Almost instantaneous initial condensation of saturated vapour on ions is followed by the sticking of the resultant charged clusters to each other. Particle growth by fusion and reciprocal neutralisation of charged clusters occurs until their size becomes of the order of the Coulomb radius $r_{\mathrm{coul}} = e^2/k_{\mathrm{B}}T$.

With a further growth of the particle radius, collision with the gas-kinetic cross-section $\sigma_{\mathrm{kin}} = \pi(r_1 + r_2)^2$ acquires greater importance as it equalises the probability for clusters bearing like and unlike charges to condense. The rate constant of this process is

$$k_{\mathrm{kin}} = \left(\frac{8k_{\mathrm{B}}T}{\pi}\,\frac{m_1 + m_2}{m_1 m_2}\right)^{1/2} \pi(r_1 + r_2)^2 \,. \tag{10}$$

For the function of cluster mass distribution $f(m) \sim \exp(-m/\bar{m})$ (where $\bar{m}$ is the mean mass of particles in a given moment), averaging yields

$$k_{\mathrm{kin}} = 10\,\frac{k_{\mathrm{B}}Tr_0}{\rho}\,, \tag{11}$$

where ρ is the mean density of the material in the condensed phase and r_0 is the mean particle radius.

The particle size increases because of the coalescence of its total mass into a drop while it is fluid. In this case, the equation for the mean particle mass $\bar{m}$ has the form

$$\frac{\mathrm{d}\bar{m}}{\mathrm{d}t} = k_{\mathrm{coag}}\bar{\rho}\,,$$

where $\bar{\rho}$ is the mean density of the material in the condensed phase and k_{coag} is the particle coagulation rate constant.

Coagulation of particles proceeds as a series of direct collisions which allows time dependence of the mean particle radius to be obtained from Eqn (11), with Eqn (10) used for the rate constant:

$$r_0 = \left(\frac{k_{\mathrm{B}}T\,\bar{\rho}^2 t^2}{4\rho^3}\right)^{1/5} \,. \tag{12}$$

Also, Table 1 lists the values of r_0 for $t = 10^{-4}$ s, that is for the time period during which the particles remain fluid. The particle radius of 10–30 nm is characteristic of a number of substances (Pt, Fe, Ag) which are formed in argon or helium at ambient pressure.

Transition of atoms to the condensed state at temperatures exceeding 1000 K is accompanied by the intensive emission of electrons from the surface which results in the formation of multicharged particles at a certain stage of system evolution.

This phenomenon is worthy of examination in more detail taking into account both electron emission and the reverse process, i.e. recombination of electrons with positively charged particles. In this case, the electron density changes at a rate of [25]

$$\frac{\mathrm{d}N_e}{\mathrm{d}t} = N\,\frac{AS}{e}\,T^2 \exp\left(-\frac{\varphi}{k_{\mathrm{B}}T}\right) - \alpha N_e N \,. \tag{13}$$

where $A = 4\pi m_e e k_{\mathrm{B}}^2/h^3$ is the Richardson emission constant (h is Planck's constant), S is the surface area of emitting particles, φ is the work function, α is the recombination coefficient, and N is the charged particle density.

$S = 4\pi r_0^2$ holds for particles with mean radius r_0. Moreover, $N_e = mN$ (m is the particle charge in electron charge units) and $\varphi = \varphi_0 + me^2/r_0$ (the term me^2/r_0 reflects increased work function due to the charge of the particle). If the recombination cross-section in the first approximation is considered equal to πr^2, then $\alpha = \pi r^2 \langle v \rangle$ (where $\langle v \rangle = (8k_{\mathrm{B}}T/\pi m_e)^{1/2}$ is the electron speed and m_e is its mass).

Substitution of expressions for S, N_e, α, and φ into Eqn (13) yields

$$\frac{\mathrm{d}N_e}{\mathrm{d}t} = \pi r_0^2 \left[\frac{4AT^2}{e} \exp\left(-\frac{\varphi_0 + me^2/r_0}{k_{\mathrm{B}}T}\right) - mN\left(\frac{8k_{\mathrm{B}}T}{\pi m_e}\right)^{1/2}\right]. \tag{14}$$

In equilibrium, $\mathrm{d}N_e/\mathrm{d}t = 0$. Hence

$$4AT^2 \exp\left(-\frac{\varphi_0 + m_0 e^2/r_0}{k_{\mathrm{B}}T}\right) = e m_0 N \left(\frac{8k_{\mathrm{B}}T}{\pi m_e}\right)^{1/2} \,, \tag{15}$$

where m_0 is the equilibrium charge of the particle.

Eqn (15) is practically identical to the relationship obtained from the analysis of equilibrium particle ionisation [26, 27] provided formation of both positive and negative charges on dispersed particles is taken into account in the latter:

$$\frac{N_e}{N} = \sigma^2 \ln\frac{K}{N_e} + \frac{1}{2}\,, \qquad \sigma^2 = \frac{rk_{\mathrm{B}}T}{e^2}\,. \tag{16}$$

Here, $K = 2(2\pi m_e k_{\mathrm{B}}T/h^2)^{3/2} \exp(-\varphi_0/k_{\mathrm{B}}T)$ is the equilibrium constant for the single ionisation reaction.

It has been shown for the case of equilibrium ionisation [26] that the charge distribution between particles is the same as the normal distribution density

$$\frac{N_m}{N} = \frac{1}{\sigma(2\pi)^{1/2}} \exp\frac{(m - m_0)^2}{2\sigma^2}\,, \tag{17}$$

where N_m is the number density (of particles with charge m) and σ is dispersion.

Table 2 presents parameters, calculated from Eqn (16), which characterise the ionisation state of plasma containing the condensed phase in the form of carbon, copper, and magnesium oxide particles. It can be seen that at the stage of condensation, particles of size exceeding 5 nm almost invariably bear positive charge of a few elementary units.

However, further cooling of the system results in the absorption of free electrons by the particles, and the charge density distribution (17) at plasma temperature below T_p becomes quasisymmetric with respect to zero; indeed, $m_0 = (N_e/N)_{T_p} < 0.1$. This implies that the densities of positively and negatively charged particles are virtually the same.

Table 2. Ionisation state of plasma containing condensed phase.

C ($T_c = 3980$ K, $N_c = 2 \times 10^{18}$ cm^{-3})			Cu ($T_c = 3270$ K, $N_c = 1.5 \times 10^{19}$ cm^{-3})			MgO ($T_c = 3870$ K, $N_c = 2.4 \times 10^{18}$ cm^{-3})		
r_0/nm	$(N_e/N)_{T_c}$	T_p/K	r_0/nm	$(N_e/N)_{T_c}$	T_p/K	r_0/nm	$(N_e/N)_{T_c}$	T_p/K
5	3.13	2840	5	0.39	3051	5	4.36	2441
10	8.32	2582	10	1.57	2738	10	10.90	2191
20	21.44	2363	20	5.75	2480	20	26.77	1996
40	53.30	2176	40	18.22	2269	40	64.21	1824

Table 3. Distribution of aerodisperse plasma particles by charge (in %) at the crystallisation temperature of the particle material ($r_0 = 15$ nm).

Material	T_{cr}/K	Number of elementary charges on the particle						
		0	1	2	3	4	5	6
C	3940	21.3	36.8	24.0	12.0	4.4	1.2	0.3
Cu	1350	36.2	47.9	14.0	2.8	0.1	–	–
MgO	3070	23.8	40.1	23.4	9.4	2.7	0.5	–

The ultimate charge distribution spectrum formed in the zone of particle-to-solid conversion is shown in Table 3.

In order to determine the time necessary to reach emission equilibrium, assume that $\varphi' = \varphi_0 + m_0 e^2/r$, $m_{t=0} = 0$ and integrate Eqn (14). This gives

$$m = \frac{4\pi r^2 A T^2}{e} \exp \frac{\varphi'}{k_B T} \, \frac{1 - \exp(-\alpha N t)}{\alpha N} \, . \qquad (18)$$

Eqn (18) suggests that equilibrium is practically reached in time $\tau = 1/\alpha N = m_0/N_e \pi r^2 \langle v_e \rangle$, where τ is an overestimate since the emission rate is minimal for the selected expression for φ'.

At $T = 3000$ K, time $\tau = 10^{-6}$ s for particles with $r = 10^{-6}$ cm, which means that equilibrium is attained if the particles remain in the zone of condensation one order of magnitude longer than is implied by the above value. Otherwise, the particle charge would be higher than the equilibrium one.

2.2 Initial stage of coagulation

An important outcome of vapour relaxation in a weakly ionised medium is conservation of a high charge by particles undergoing transition to the solid state. Owing to this, the early stage of coagulation largely occurs between charged particles. This predetermines to a large extent both the growth mechanism and the structure of the primary clusters.

Numerical models of charged solid particles with the Coulomb interaction potential provide a clear idea of principal features of the system evolution at early stages of aggregation. Specifically, calculations by the Monte Carlo method indicate that thermodynamic parameters of an ionic system in gaseous phase should not be regarded as smooth functions of temperature and pressure; indeed, they show peculiar characteristics which suggest the existence of phase transition at selected points.

Typical relationships calculated for the internal energy of a system of 12 charged particles with a rigid kernel are illustrated in Fig. 1 [28]. The figure shows that high density isochores exhibit four segments of smooth, almost linear energy behaviour separated by characteristic steps.

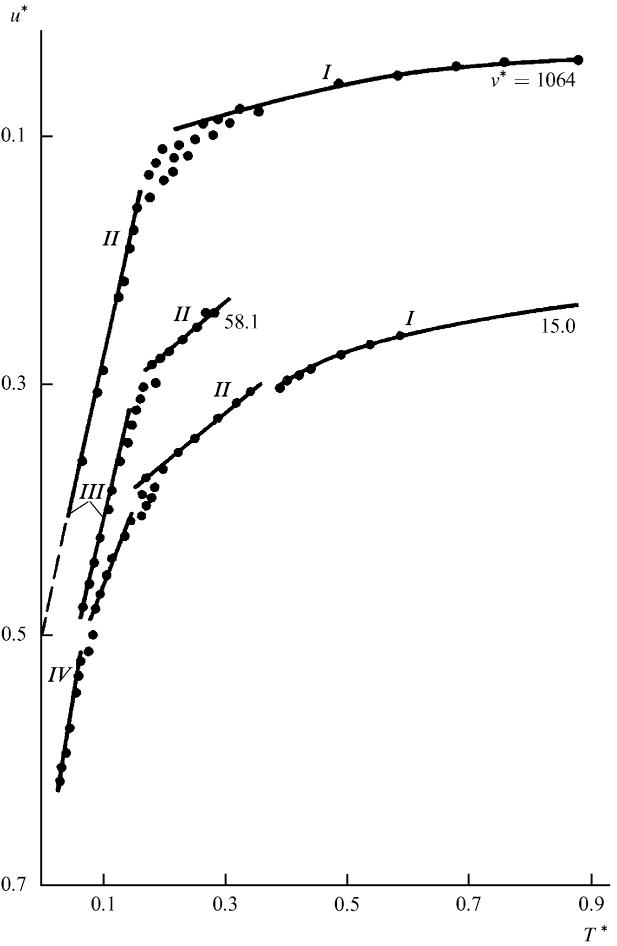

Figure 1. The plot of internal energy u^* (per particle) vs temperature T^* at different density of the particles in the system. Dimensionless parameters are used: $u^* = u/\varepsilon$, $T^* = T/\varepsilon$ where $\varepsilon = m^2/2r_0$, $v^* = v/(2r_0)^3$.

Analysis of binary distribution functions and instantaneous configurations corresponding to the points at each of the above segments permitted their identification with various types of structures. The high-temperature segment *I* ($T^* > 0.38$) corresponds to the Debye region of isolated charges. The temperature range *II* ($0.17 < T^* < 0.38$) is associated with the formation of ion pairs, whereas segment *III* ($0.08 < T^* < 0.17$) corresponds to increasing triple correlations and tends to produce linear ion triplets.

The next step following the formation of triplets is the build-up of long chains rather than production of compact ion quadruplets. In this process, the high-temperature portion of segment *IV* ($0.05 < T^* < 0.08$) corresponds to the region where chains are assembled. In the low-temperature portion $T^* < 0.05$, the chains are folded into compact structures.

Table 4. Temperature intervals (in kelvins) for different structural types of charged particles calculated for solid particles with density 10^{15} cm^{-3}.

Type of structure	The number of elementary charges on the particle					
	1	2	3	4	5	6
Single charges	> 210	> 845	> 1900	> 3380	> 5290	> 7610
Ion pairs	95–210	380–845	850–1990	1510–3380	2360–5290	3400–7610
Triples	45–95	180–380	400–850	710–1510	1110–2360	1600–3400
Chains	28–45	110–180	250–400	450–710	650–1110	1000–1600
Folded chains	< 45	< 110	< 250	< 450	< 650	< 1000

This can be accounted for by the fact that transition to compact structures in a system of particles of unlike charge is not accompanied by such a dramatic energy drop as in the case of neutral particles; aggregation brings together both like and unlike charges.

Chain formation is entropically favourable. The free energy $F = U - TS$ becomes crucial only at a much lower temperature, and this results in the transition of the system to a compact structure. This inference is confirmed by calculations using harmonic approximation [29] which reveal a broad region $(0.02 < T^* < 0.06)$ of thermodynamic stability of chain-like clusters on the phase diagram.

Furthermore, analysis of a number of locally stable configurations demonstrated that chains are a typical but not the sole variant of the chain structure. As the aggregate size grows, 'cross-linking' of isolated chains into branched structures becomes entropically more favourable.

The results of numerical models are largely supported by experimental findings. To facilitate their comparison, Table 4 shows temperature intervals for different types of structures in relation to the particle charge.

Formation of primary pairs and triplets can be seen on micrographs of carbon clusters obtained at high magnification. Fig. 2a demonstrates that primary structure-forming

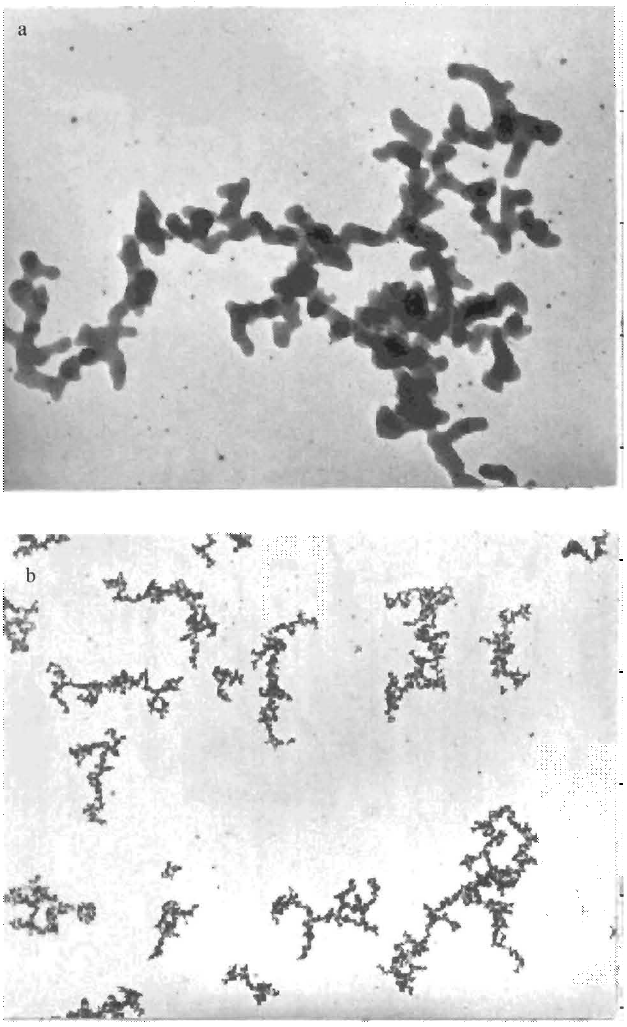

Figure 2. Micrographs of carbon clusters: (a) a fragment of aggregate structure (×70 000), (b) cross-linked filamentary structures (×7 000).

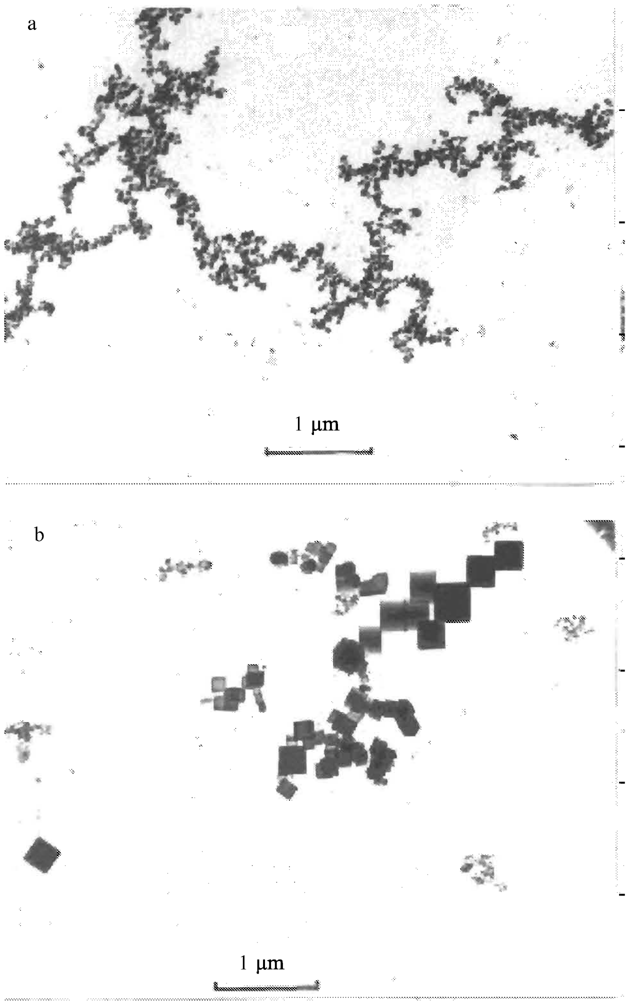

Figure 3. Aggregates of magnesium oxide obtained by burning magnesium: (a) in arc discharge, (b) in air.

elements of the cluster are linear aggregates rather than isolated kernels. Each aggregate consists of two or three particles, and their combination at an early stage of aggregation gives rise to both filamentary and 'cross-linked' structures (Fig. 2b).

Another characteristic indicator of the relationship between the ionisation state of a system and the structure of aggregates is provided by a comparative study of burning magnesium in arc discharge and in air (Fig. 3). In the first experiment magnesium was burnt in a plasma channel at 10 000 K whereas in the second experiment the combustion temperature did not exceed the magnesium oxide condensation temperature, i.e. 3000 K [30].

In arc discharge, ionisation equilibrium was grossly disturbed at the time of vapour condensation, and primary ion number density was much higher than equilibrium density. This accounted for a large amount of small particles formed during condensation. High initial particle density in a fixed temperature range was responsible for markedly reduced energy of chain formation (see Fig. 1) and therefore an increased relative density of chain-like structures.

Burning of magnesium oxide in air had quite a different outcome. In this case, magnesium oxide vapour condensed on a relatively small amount of ions which accounted for the low particle number density and a much weaker tendency for the particles to form. An additional factor which interfered with chain formation during burning of magnesium oxide in air was the relatively large size of primary particles (around 0.2 μm). Diffusional movements of such particles partly counterbalance the directional effect of coagulation produced by the Coulomb interaction forces.

Thus in the early stage of particle coagulation, which as a rule occurs in the gas-kinetic regime, the ionisation state of the medium has a major effect on the structure of primary clusters. Results of numerical models and experimental findings both indicate that chain-like structures are most readily formed in high-temperature systems with initially enhanced density of charged particles.

Given equal particle densities, chains are most likely to form in the case of substances with high melting point whose particles carry higher charges during conversion to solids. Such conditions are characteristic of plasma media generated by arc discharge or laser vaporisation of refractory materials. It is in these systems that chain aggregates are most frequently found as both linear and ramified structures.

2.3 Late coagulation. Effect of electric field

Further growth of aerodispersed particles giving rise to fractal clusters occurs from the previously formed small aggregates that tend to fuse into bigger structures, i.e. by the mechanism of cluster – cluster aggregation.

This process comprises two stages differing in physical mechanisms and hence in characteristic times. In the first stage, particles draw together till they touch one another (diffusion); during the next stage, particles that are in contact join together via intermolecular bonds. Based on the different characteristic times of the two processes, models of cluster – cluster aggregation are categorised into two major types: diffusion-limited aggregation (DLA) and reaction-limited aggregation (RLA).

In RLA, the 'binding' time of particles greatly exceeds the characteristic time needed to bring them together. In other words, each particle is involved in a few collisions before an aggregate is produced. This ensures deeper interpenetration of the particles and formation of compact structures. According to Refs [31, 32], the characteristic fractal dimension of such aggregates is $D \approx 2.1$.

In DLA, diffusion of particles takes more time than their 'binding' which means that each collision results in aggregation. In this case, interpenetration of the particles is not so deep as in RLA and the fractal dimension of the resulting aggregates is smaller: $D \approx 1.78$.

The type of aggregation that is actually produced depends on the properties of the dispersed system, i.e. its density, materials of the dispersed phase and the medium, the number, size, and charge of the particles. It follows from the foregoing discussion that at an earlier stage of aggregation, the cluster growth largely occurs in accordance with the RLA model owing to the high density of small dispersed particles and, hence, increased frequency of their collision. The particle number density decreases as more primary aggregates are formed, and their further growth is limited by the diffusion rate.

In fact, the majority of real aggregation processes are far more complicated because they include reorientation of the constituent components inside clusters (restructuring), chemical reactions on their surface, breakdown of the established links, etc.

An important feature of the cluster – cluster aggregation is its susceptibility to the presence of external fields. This accounts for the structural anisotropy of the clusters being formed. This effect should be attributed to the orientation of the clusters in the external field where their aggregation proceeds in a certain preferred direction.

Electric fields appear to be of special interest in this context, and their influence on cluster aggregation has been examined in a number of experimental studies. In an electric field E, aerosol particles are subject to polarisation, and the induced dipole moment for nonspherical particles is dependent on their orientation with respect to the electric field lines. The induced dipole moment for elongated aerosols (e.g. chains of primary kernels) can have the form

$$p_{\mathrm{ind}} = \kappa E \cos\theta \,, \tag{19}$$

where κ is polarisability of the aerosol (proportional to the particle length) and θ is the angle between the particle axis and the electric field.

Moreover, primary aggregates formed at an early stage of coagulation may have their own dipole moment since they mostly arise from oppositely charged particles; the direction of this dipole moment more or less coincides with that of the aggregate axis. Interaction of the induced dipole moment and the dipole moment of the aggregate with the electric field causes the aerosol particles to assume the most energetically favourable orientation, i.e. along the electric field lines.

Particle distribution in terms of orientation with respect to an electric field can be found by using the Boltzmann law [33]:

$$f(\theta) \sim \exp\left[-\frac{(\kappa E \cos\theta + p_0)\,E\cos\theta}{k_{\mathrm{B}}T}\right] . \tag{20}$$

It is clear that the fraction of oriented particles increases with increasing electric field.

The average cosine of angle θ may be used as a measure of particle orientation in an aerodisperse system. $\overline{\cos\theta} = 0.5$

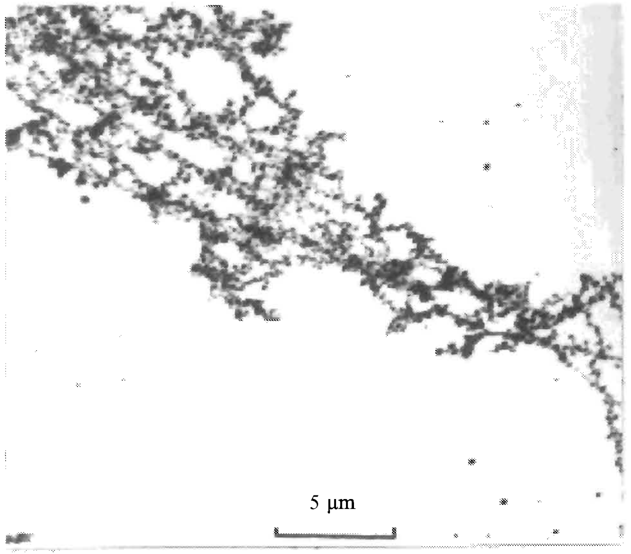

Figure 4. Representative fragment of the structure of an anisotropic fractal carbon cluster grown in an electric field of 2.5 kV cm^{-1}

corresponds to the absence of regular orientation whereas $\cos\theta = 1$ indicates that all the particles are oriented along the field lines.

Calculations show that elongated aggregates (0.1 μm) are completely oriented ($\overline{\cos\theta} \geqslant 0.9$) at ambient temperature in an electric field of around 1 kV cm^{-1} whereas orientation of chains 1 μm long occurs in a field as weak as 30 V cm^{-1}. Therefore, this effect is apparent only when the temperature of the system is not too high. Otherwise, thermal motion prevails over the directional effect of the electric field.

Another aspect of the influence of the electric field on coagulation is related to the directional drift of particles along the field lines caused by the uncompensated charge they carry. Moreover, the effect of dipole–dipole interaction between polarised aggregates becomes more and more pronounced as they draw together which results in faster aggregation of clusters.

All the above factors are collectively responsible for the formation of highly anisotropic elongated fractal clusters, and anisotropy is equally inherent in the inner structure of the aggregate. A representative fragment of such a structure is presented in Fig. 4.

In strong electric fields (ca 100 V cm^{-1}) and at a high initial particle density, directional cluster–cluster aggregation may result in the formation of macroscopic structures called fractal threads (filaments) [13]. Electric field is of paramount importance in the formation of such structures; apart from the factors mentioned above it contributes to the consolidation of cluster structure, in agreement with the restructuring model [34].

Thus, fractal threads can be considered as the final result of directional cluster–cluster aggregation in an external field. In isotropic conditions, aggregation of the cluster–cluster type is directionless and leads to the formation of isotropic loosely bound aggregates. The eventual outcome of this process is a single macroscopic cluster, i.e. an aerogel.

3. Experimental studies on growth dynamics of fractal aggregates

3.1 Experimental design

It has already been mentioned that experiments on fractal cluster generation normally begin with evaporation of the starting material by one of the available techniques. This procedure is followed by vapour condensation which results in the formation of dispersed primary nanometer particles; their further aggregation gives rise to larger aerodisperse agglomerations. The structure of such aggregates will be the subject of the following discussion.

The experimental setup was designed to grow fractal clusters in line with the above scheme [20]. It consisted of three basic modules: a generator of particles, a coagulation chamber, and a sampling unit (Fig. 5).

The main element of the generator was the passive evaporator *1* with cooled walls. The material was heated by means of tube heater *2* and cooled by pumping gas (W_3) through the evaporator. Vapours were mixed with a flow of nitrogen (W_1) at the entrance of the generator.

The gas mixture was heated to 1000 K then passed to condensation chamber 3 where it was further mixed with cold gas (W_2) which resulted in a sharp drop of vapour temperature to 400 K and its condensation. The design of the apparatus allowed the number density of primary

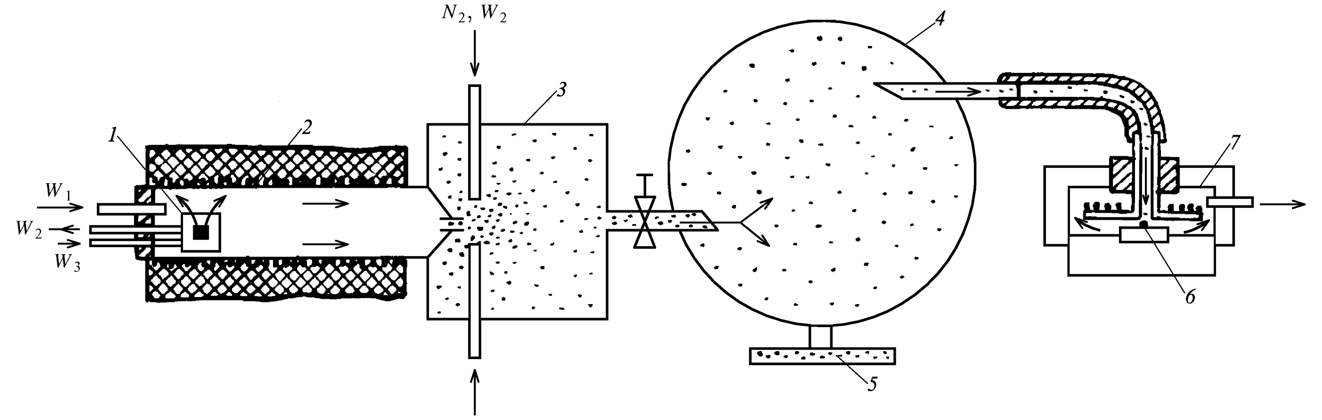

Figure 5. Diagrammatic representation of the experimental setup for growing fractal clusters. The notation is explained in the text.

particles at the outlet of the generator to be changed over a broad range by varying only the melting temperature. This did not seem to affect the size of the resulting particles appreciably (20–40 nm).

Particles aggregate in coagulation chamber *4*, a 20 litre isothermal brass sphere which admitted the outside air through multilayer filter *5*. Measurement of the coagulation time started as soon as the chamber volume was assumed to be filled to the desired density. Aggregated particles were deposited on substrate *6* in thermal precipitator *7*.

The operating parameters of the generator were chosen to ensure filling the chamber volume to the required initial particle number density (ca 10^6 cm^{-3}) within 2 to 3 min. In this case, characteristic growth time was about 1.5 h. Sampling performed within the scheduled time-frames allowed evolution of the system to be traced from the formation of primary aggregates until micrometer clusters had been produced.

We normally used lead iodide (PbI_2) as a starting material to obtain fractals. This compound is known to be readily converted to a vapour and, besides, provides the necessary image contrast in an electron microscope.

It should be emphasised that electron microscopy is universally applied to the structural analysis of micrometer and submicrometer clusters. Statistical treatment of the microscopic findings allows a number of geometric parameters of individual clusters and ensembles of aggregating particles to be obtained.

Application of such analysis to images obtained at different points in time made it possible to trace the evolution of the aggregation system in some detail and revealed mechanisms responsible for the formation of fractal cluster structures.

3.2 Morphological analysis of aerosol clusters

Geometric analysis of visual images is one of the most widely used methods for studying fractal properties of different objects. Depending on the size of the object, it may be viewed either directly (photographic and television images) [35, 36] or with the use of light [37] and electron [15] microscopy. Brightness in different points of the image indicates whether they belong to the object or not.

Further analysis of the image for the purpose of revealing clues about fractals requires first of all its discretisation. This procedure divides the image (photograph, TV image, etc.) into a finite number of constituent elements, each considered to be uniformly bright.

In this way, an initially continuous planar image is divided into a number of discrete elements organised in a rectangular grid. The minimum size of an element l_0 depends on the resolution of the scanner and in turn determines the quality of fractal analysis.

Ideally, the size of an image element l_0 should be the same as the size r of the primary particles which give rise to the aggregate and the frame size compatible with the size of the examined aggregate. Moreover, the number of discrete elements must be sufficiently large (of the order of 10^4) to enable scale invariance of the cluster to be verified in a wide size range.

Image discretisation reveals areas corresponding to fractal clusters, and further processing of the image is performed by means of standard algorithms, in accordance with the theory of fractal systems.

To begin with, characteristic cluster size or radius of gyration R_g can be determined as the average quadratic distance between elements in the cluster. This parameter is most convenient for isotropic particles [38]:

$$R_g^2 = \frac{1}{2N^2}\sum_{i,j=1}^{N}(\boldsymbol{r}_i - \boldsymbol{r}_j)^2 = \frac{1}{2N^2}\sum_{i,j=1}^{N}\left[(x_{1i}-x_{1j})^2 + (x_{2i}-x_{2j})^2\right], \quad (21)$$

where N is the number of cluster elements in the image, $\boldsymbol{r}_k$ is radius vector of the k-th element, x_{1k} and x_{2k} are the Cartesian coordinates of this element.

In the case of anisotropic aggregates, all components of the tensor of inertia need to be determined to obtain a qualitative description of the degree of anisotropy:

$$R_{mn}^2 = \frac{1}{N}\sum_{i,j=1}^{N}(x_{mi}-x_{mj})(x_{ni}-x_{nj}), \quad (22)$$

where $m, n = 1, 2$ (for a flat image).

Diagonalisation of the tensor (22) gives the main radii of gyration, $R_1 \leqslant R_2$,. Their ratio is a measure of fractal cluster anisotropy [37, 39]:

$$A = \frac{R_1^2}{R_2^2}. \quad (23)$$

A major feature of fractal objects is self-similarity of their internal structure which can be qualitatively characterised by the fractal dimension D, obtained from relation [38]

$$N \propto R^D, \quad (24)$$

where N is the number of primary particles which constitute the fractal aggregate, within a sphere of radius R. For practical purposes, the number of cluster elements in the image N_0 is counted within a square grid of area $L \times L$ with the centre coincident with the cluster mass centre.

Given self-similarity of the aggregate structure, the plot of N_0 vs L in logarithmic coordinates is a straight line, the slope of which defines the fractal dimension commonly referred to as mass fractal dimension

$$D = \frac{\mathrm{d}\left[\ln N_0(L)\right]}{\mathrm{d}(\ln L)}. \quad (25)$$

However, the law of similarity is valid only on scales $l_0 \ll L \ll R_g$. For this reason, the fractal dimensionality described by Eqn (25) largely depends on the choice of fractal interval boundaries.

Mathematically, such a problem is ill-posed, and the minimum error criterion for D cannot be used for the optimal choice of this fractal interval. Hence, the likelihood of the mass fractal dimension being greatly in error. This fact was considered in Ref. [40] where the notion of 'cell' fractal dimension D_b was suggested as allowing for more correct calculation.

Evaluation of 'cell' fractal dimension is possible by covering a given fractal set with a lattice of equally-sized squares [41]. The number of filled squares N_b is related to their size ε by the law of similarity:

$$N_b(\varepsilon) \propto \varepsilon^{D_b}. \quad (26)$$

For a strictly self-similar fractal, cell and mass dimensions coincide, but comparative calculations performed for real fractal clusters [42] indicate that cell fractal dimension exhibits a smaller spread of sizes which makes it preferable for the description of fractal properties of aggregated particles.

This approach may be employed to determine the dimensions for a selected class of fractals. Assuming identity of structural characteristics of clusters in an aerodisperse system (as the clusters grow under similar conditions) and using relation (24), one can extrapolate observations on individual clusters to the law of similarity for the entire assembly of particles, as follows:

$$N \propto R_{\mathrm{g}}^{D_\beta}\,, \tag{27}$$

where N is the number of elements in a cluster of size R_{g}.

Fractal dimension D_β can be determined by measuring the radius of gyration R_{g} and N for a large number of aggregates in the system. On the one hand, the aggregates thus examined must contain many primary particles (i.e. they must be fractal aggregates). On the other hand, these aggregates must be significantly different in terms of size so that D_β can be found from the dependence $\ln N(\ln R_{\mathrm{g}})$ with a sufficient degree of accuracy.

These requirements are somewhat contradictory and can be fulfilled only at later stages of coagulation in an aerodisperse system when clusters undergo extensive distribution by size.

The foregoing discussion has demonstrated that fractal image analysis requires bulky calculations which are greatly facilitated by the use of computers. A large variety of devices is currently available to solve the main technical problem, i.e. loading an image on the computer. Most of these instruments is scanners of various types for loading images from paper carriers (photographs, etc.) [42] or the so-called framegrabbers for loading directly from a videocamera [37].

Discretisation of primary images is accomplished as they are loaded into the computer memory. These devices are useful in automation of fractal analysis and processing of large volumes of experimental data.

3.3 Fractal dimension and the structure of growing clusters

Complicated and multistep patterns of coagulation growth of clusters involving different stage-specific physical mechanisms to a large extent dictate the methods for studying the dynamics of this phenomenon. Experimental studies have demonstrated that a very characteristic feature of the aggregate formation is the relationship between the structural parameters of the clusters and the duration of their growth.

Evolution of fractal dimensions and the cluster radius of gyration in time is found to provide most information for the analysis of relaxing aerodisperse systems. This conceptual approach was applied to experiments in which fractal clusters were grown and their properties analysed together with those of aerogels obtained from these clusters. Selected results of this study are discussed below.

The method used to grow and analyse $\mathrm{PbI_2}$ clusters as described in Section 3.1 was also employed to elucidate the dependence of D_α and D_β on the time of coagulation and the initial particle density (Fig. 6). Taken together, results of kinetic analysis and electron micrographs of the aggregates [20] allowed the correlation of changes in the values of D_α and D_β seen in the plots with structural changes in the growing aggregates. Specifically, it has been shown that in the beginning prior to the onset of aggregation, their planar projection gave values of $D \approx 2$.

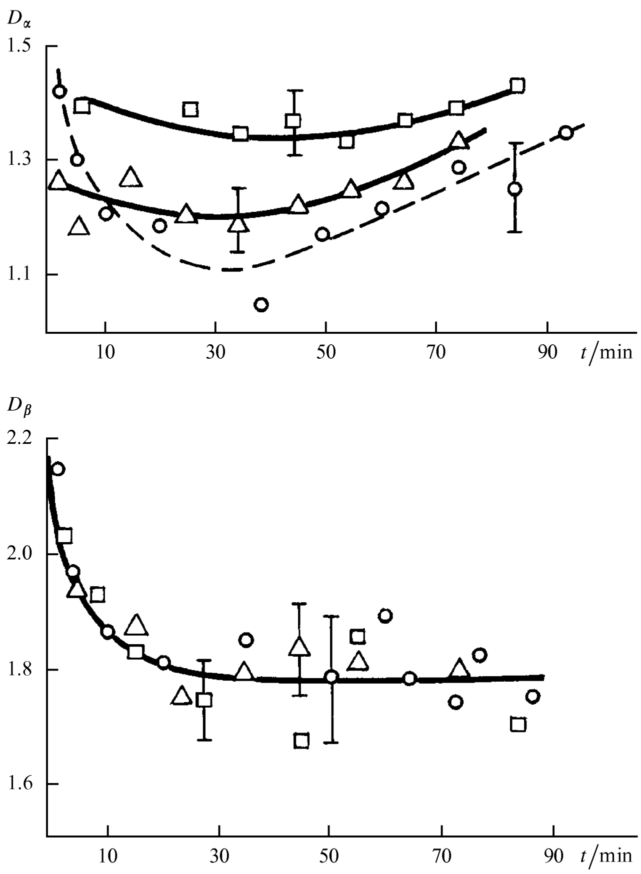

Figure 6. Plots of D_α and D_β versus coagulation time t at initial particle densities ($\mathrm{cm^{-3}}$) of 4×10^5 (circles), 10^6 (triangles), and 2×10^6 (squares).

Aggregation normally started as cluster–particle interaction. The plots exhibit a characteristic decrease in fractal dimension associated with the formation of primary clusters with anisotropic structure at an early stage of the process.

For uncharged particles, growth anisotropy is largely due to the effect of particle polarisation immediately before collision [43]. Nevertheless, we believe that the influence of charges on the formation of such structures cannot be totally excluded because some of them appear to carry a charge even at room temperature [see Eqn (17)].

As more monomers are bound in clusters at later stages, the cluster–particle interaction gives way to the cluster–cluster mechanism of aggregation which leads to a gradual decrease in growth anisotropy and, in the end, to the production of relatively symmetric fractal structures with higher D values.

It is worthwhile to note that fractal dimension is generally assessed for bigger aggregates on scales which considerably exceed the size of the primary particles. In this size range, the structures are self-similar, and their fractal dimension is the same as their similarity dimension [38]. At the same time, fractal dimension D based on the Hausdorff–Besicovitch formalism can be determined just as well for the systems that do not possess such a property.

An example of such systems is provided by clusters formed at an early stage of growth and composed of tens of particles. There is evidence that the fractal dimension of such aggregates remains very useful in that it serves as a quantitative characteristic of the filling by the cluster of the space it occupies.

Comparison of the dependences in Fig. 6 reveals that the absolute values of D_α and D_β do not coincide in the entire range of coagulation times examined in the present experimental study. This disagreement is largely due to changes in cluster structure near its boundary. For this reason, specific features of fractal growth near the outer boundaries must be taken into consideration when comparing dimensions D_α and D_β.

Refs [44, 45] introduce the notion of the outer active zone (penetration depth) Δr which collects all the newly incoming monomers. In the case of Gaussian probability of their joining the cluster, the relation between D_α and D_β may be written in the form [46]

$$D_\alpha = D_\beta \left[1 + \left(\frac{2}{\pi} \right)^{1/2} \frac{\Delta r}{R} \right] . \tag{28}$$

We used expression (28) to calculate the dependence of Δr on cluster size (R_g). Fig. 7 shows that penetration depth of the particles increases in an almost linear fashion with increasing cluster size. This feature of the aggregate growth appears to be typical of early coagulation stages where clusters are represented by very loose structures.

On introduction of the relationship $\Delta r \sim R^\gamma$, data from Fig. 7 yield $\gamma = 0.86 - 0.96$. According to Ref. [46], $\gamma = (d - D_\alpha)/2$, where d is the space dimensionality. It is easy to see that a similar result can be obtained by substituting experimental values of D_α into this expression.

Also, Fig. 7 suggests that the dependence of penetration depth on the cluster size ceases beyond a certain value of R_g (which in turn depends on the monomer number density). Associated with this size range is a coagulation stage at which the bulk of the primary particles join together upon contact to form clusters. At this stage of the evolution of the system, the cluster–cluster mechanism of aggregation is predominant. This strikingly decreases the probability of cluster interpenetration which in turn results in the termination of active zone growth. This observation is supported by the value of fractal dimension $D_\beta = 1.75 \pm 0.08$ reached within 40 min after the beginning of coagulation. This is characteristic of cluster–cluster aggregation of Brownian particles [32].

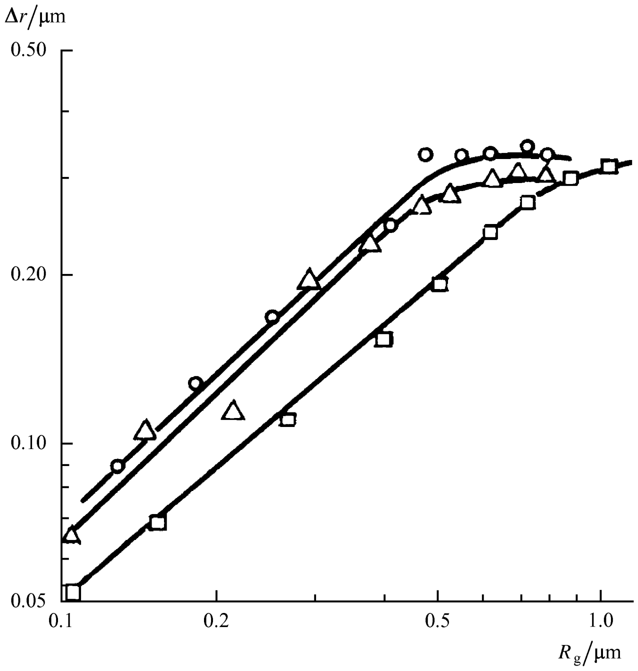

Figure 7. Relationship between cluster size and penetration depth. See Fig. 6 for notation.

3.4 Scaling in the course of growth

Self-similar aggregates are not the sole product of cluster–cluster aggregation. The process also results in a scaling (i.e. self-similar) distribution of cluster size.

Coagulation growth dynamics of aerodispersed aggregates can theoretically be described with the use of the Smoluchowsky equation in the discrete form [47] which takes into account evolution of the cluster size distribution function in time. If the kernel of the coagulation equation is a uniform function of its arguments, an aerodisperse system may 'forget' its initial state after a certain transition period and tend to evolve towards the self-similar particle size spectrum.

According to Ref. [48], the cluster size distribution function can be well represented by the following scaling form:

$$C_s(t) \sim t^{-\omega} s^{-\tau} f\left(\frac{s}{t^z} \right) , \tag{29}$$

where C_s is the density of the number of clusters containing s primary particles, t is coagulation time, and $f(x)$ is a universal function independent of the initial distribution which satisfies conditions

$$f(x) \to 1 , \quad x \ll 1 ,$$

$$f(x) \to 0 , \quad x \gg 1 .$$

A novel feature of the distribution function $C_s(t)$ is the presence of two dynamic exponents ω and z in addition to the usual static exponent τ. The exponent ω describes the power-law decay of the number density of the cluster with time during aggregation for the entire range of cluster sizes, whereas exponent z governs the growth of the mean cluster size S in the system:

$$S(t) = \frac{\sum C_s(t)\, s^2}{\sum C_s(t)\, s} \sim t^z . \tag{30}$$

Scaling exponents of distribution function (29) are not independent. The similarity relation cited in Ref. [48] is fulfilled for them in the form of

$$\omega = (2 - \tau) z . \tag{31}$$

Experimental verification of scaling laws was performed on a lead iodide aerosol with primary particles of 20–40 nm. The initial aerosol number density in the system varied in the range of $(0.4 - 1.8) \times 10^6$ cm^{-3}. The results of evaluation of the cluster size distribution at different times after the start of aggregation are summarised in Fig. 8.

The plot in Fig. 8 illustrates the dependence of the integral cluster number density

$$\Delta N_s = \int_s^\infty f(x)\, \mathrm{d}x$$

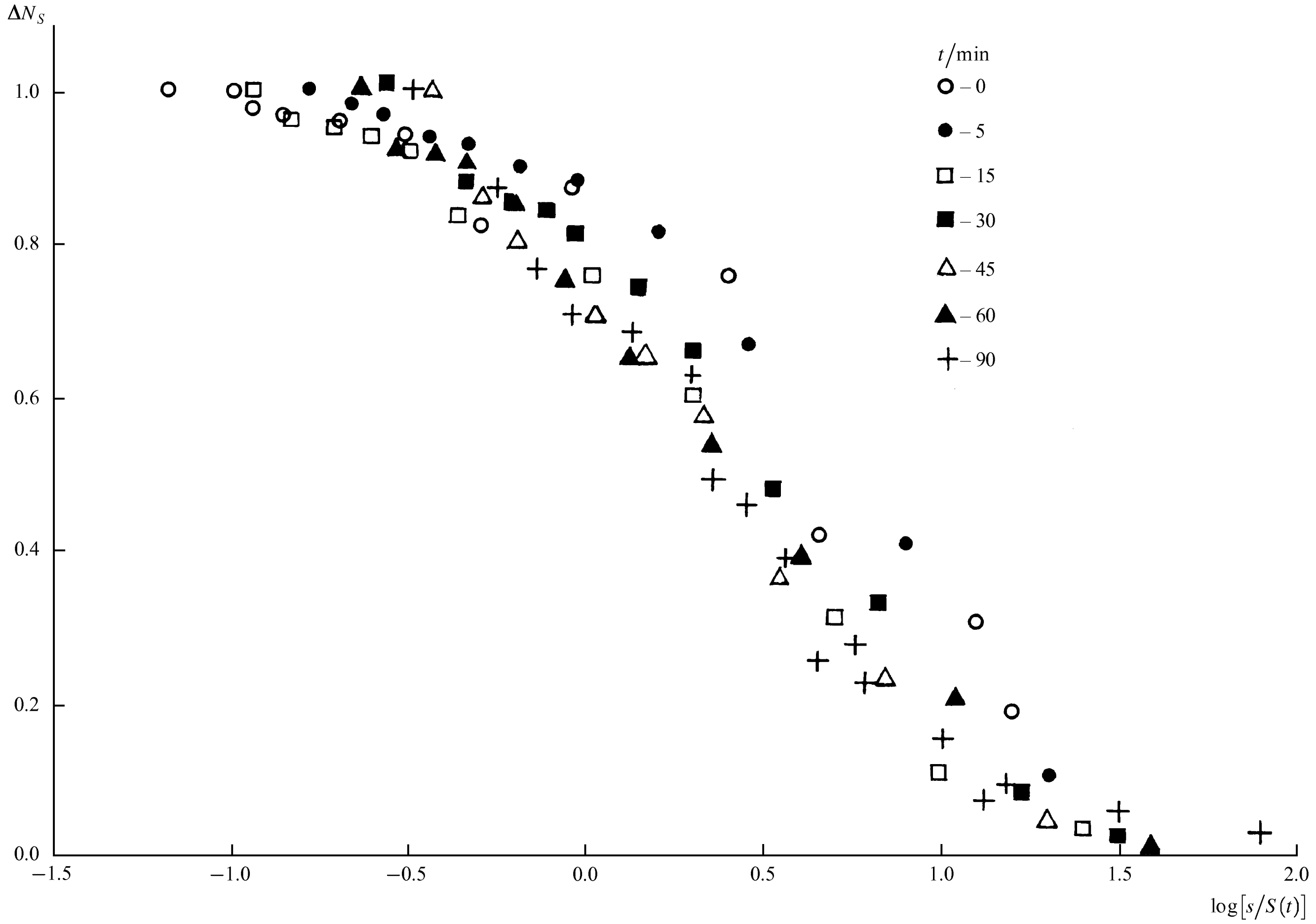

Figure 8. Scaling PbI_2 cluster size distribution at different time-points after the initiation of aggregation.

on relative size of the clusters, $s/S(t)$. It can be seen that almost all experimental data taken at different times during the coagulation process fall approximately on a single curve. This suggests scale invariance of the size spectrum.

To determine scaling exponents from experimental findings, it is necessary to specify the shape of the self-similar function $f(x)$. Asymptotic analysis of the solution of the coagulation equation for homogeneous kernels gives exponential behaviour of the scaling function for large x [49].

This in turn allows the function of cluster size distribution to be represented in the form

$$C_s(t) \sim t^{-\omega} s^{-\tau} \exp\left[-\frac{s}{S(t)}\right]. \tag{32}$$

Eqn (32) was used to determine scaling exponents ω, τ, and z, from the experimental values of the scaling exponents $C_s(t)$ and $S(t)$. They turned out to be close for all initial particle densities in the system, i.e. $\omega = 0.44 \pm 0.08$, $z = 1.1 \pm 0.3$ and $\tau = 1.62 \pm 0.18$. Evidently, scaling exponents thus obtained satisfy the similarity relation (31) (within analytical error limits) which confirms the validity of the scaling form of the cluster size distribution function.

Moreover, because the aerodisperse system has a self-similar size spectrum, it is possible to find the fractal dimension D_β. Indeed, it follows from the definition of fractal dimensions that

$$S(t) \sim R_g^{D_\beta}. \tag{33}$$

Comparison of this expression with Eqn (30) yields, in the scaling approximation,

$$R_g \sim t^{z/D_\beta}. \tag{34}$$

Therefore, knowing the scaling index z and using dependence $R_g(t)$, one can calculate the fractal dimension; in the present experiment it was found to be $D_\beta = 1.7 \pm 0.3$.

It is concluded from the results of this experiment that the evolving aerodisperse system displays scale invariance, with scaling taking place very early during coagulation.

The scaling parameters found by experiment satisfy the similarity relation (31) but at the same time differ substantially from those obtained by computer modelling [50]. This discrepancy suggests a more complicated physical mechanism underlying the real process of particle aggregation than the one predicted by mathematical models of cluster growth.

4. Gas-dynamic and sorption properties of fractal aggregates. Effect of structure

4.1 Principles of cluster structure modification by the electric field

Theoretical considerations indicate that fractal clusters must possess interesting and unusual (compared with continuous particles) physical properties. Specific features of their structure are exposed in modelling their optical [51, 52, 53], aerodynamic [10, 11], and sorption [54, 55] properties. Unfortunately, experimental studies in this field are largely nonexistent. One reason for the lack of substantial progress in this area is the difficulty of obtaining, from the same substance, aggregates with different fractal geometry.

An approach to the solution of this problem is provided by the method of structural modification based on the effect of surface tension forces. The simplest way to employ this approach is to pump a gas-dispersed system through a tubular furnace where surface tension forces at high temperature gradually consolidate aggregate structures with a concurrent increase in fractal dimension. For example, experiments with silver aggregates revealed enhancement of D from 2.06 to 2.18 when the temperature inside the furnace is increased from 290 K to 390 K [56].

A similar effect of surface tension forces on the cluster structure was demonstrated in experiments on capillary condensation of water vapour [8]. Fractal soot particles with the initial dimension $D = 1.78$ were shown to become gradually more densely packed under the effect of surface tension forces of the condensate, which accumulated in pores. Finally, at a 3% supersaturation, water filled up all the pores. The droplet thus formed compressed the particle so that it turned into a dense globule of dimension $D = 2.5$.

Another approach to the solution of the problem of structural modification of aggregates is based on the effect of directional particle coagulation in the electric field (see Section 2.3). This approach is essentially different from the previous one in that it uses assemblage of the constituent elements under controlled conditions rather than deforming compaction of them.

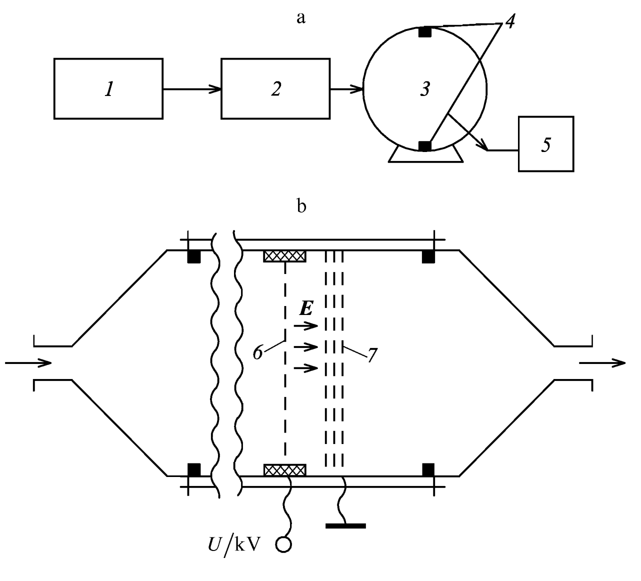

Figure 9. The experimental system for obtaining fractal clusters in the electric field: (a) functional block diagram, (b) a single cascade of the electrodiffusion separator. See the text for notations.

With this approach, the aggregate structure strongly depends on the shape of the primary clusters. Specifically, at the terminal stage of evolution, filamentous clusters have been shown to give rise to very loose structures of very low density with $D \sim 1.3$ [57].

An example of practical application of the directional growth technique is described below. The experimental setup used in our study was equipped with an electrodiffusion separator of particles *2* (Fig. 9a), placed between particle generator *1* and coagulation chamber *3*.

The electrodiffusion separator is a modified version of the diffusion trigger battery (Fig. 9b) where each individual cascade has an additional gauze electrode *6*. Voltage U of up to 8 kV is applied between the electrode and grids *7* (cell size 1 mm). The optimal number of cascades and grids is selected empirically.

During the flow of the aerodisperse system through the cascades of the separator, the particles preferentially coagulated along the electric field $\boldsymbol{E}$ giving rise to primary clusters with prominent shape anisotropy. Isolated kernels that failed to react because of high diffusive mobility accumulated on the grids in the separator. As a result, the flow at the outlet of the separator contained a large number of small clusters and with minor fraction of free kernels (Table 5). Further aggregation (largely of the cluster–cluster type) proceeded in the coagulation chamber.

Samples were collected from the coagulation chamber at different times with the aid of thermal precipitator *5* (Fig. 9a) which allows us to follow the effect of preliminary modification on the structure of fractal clusters during their growth. Fractal dimension D_α is plotted in Fig. 10 as a function of the radius of gyration R_g in relation to the parameters of the initial dispersed system listed in Table 5.

Fig. 10 shows that the fractal dimension and hence the cluster structure change in the course of growth. Curves $D_\alpha(R_g)$ can be divided into two parts.

The first part corresponds to the small-sized range of particles and shows a decrease in D_α. This is common for all three plots and is due to the formation of structures with prominently anisotropic shape at early growth stages. The second part, at $R_g \geqslant 1.5$ µm, clearly reflects the effect of the initial parameters of the dispersed phase on the aggregate structure produced in the course of coagulation.

It is seen from Fig. 10 that the association of particles previously modified in the separator gave rise to very loose structures with low D_α values whereas unaltered particles (curve *1*) grew into compact clusters of greater fractal dimension.

Characteristically, for modified particles which aggregated at high $P_{\text{cl-cl}}$ values, there was a transition from scaling invariance of the internal cluster structure

Table 5. Characteristics of primary clusters at the exit of the electrodiffusion separator.

Field tension E/kV cm^{-1}	Number of cascades	Curve number, Fig. 10	Mean linear size $L_{\max}$/µm	Shape anisotropy $L_{\max}/L_{\min}$	Relative amount of monomers	Initial probability of cluster–cluster aggregation $P_{\text{cl-cl}}$
0	0	1	0.18	1.40	1.47	0.28
6	1	2	0.27	1.75	0.18	0.67
6	3	3	0.48	2.17	0.04	0.92

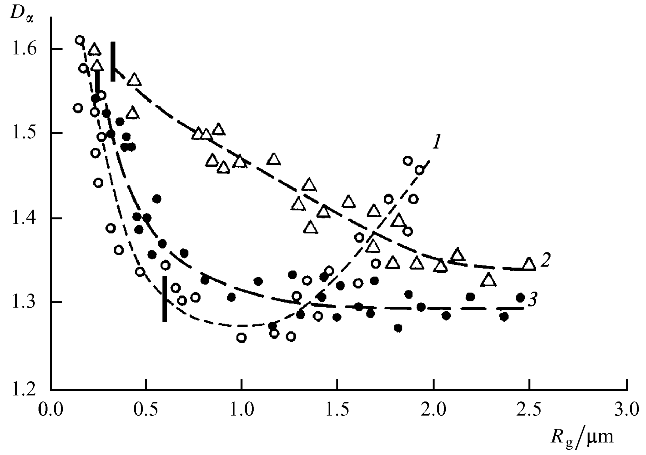

Figure 10. Relationship between fractal dimension D_α and the gyration radius R_g of the clusters. Curves *1–3* correspond to parameters of the dispersed system listed in Table 5. Vertical bars are boundaries where the system undergoes transition to cluster–cluster aggregation ($P_{\text{cl–cl}} = 1$).

$[D_\alpha = f(R_g)]$ to self-similarity of the entire set of aggregating particles (D_α = const), within the coagulation times investigated in the present experiment. In this case, the higher $P_{\text{cl–cl}}$ was the sooner the system entered the automodelling region.

4.2 Gas dynamics of fractal clusters and aerogels

Structural modification was even more apparent in investigations into aerodynamic properties of aggregates. These properties were studied by measuring the gravitational sedimentation rate of the particles.

The sedimentation rate of the particles in coagulation chamber *3* was evaluated with the aid of two collecting elements (Fig. 9a) designed to capture precipitated particles. The additional collector placed in the top portion of the chamber was necessary to make up for potential biases in the size and density spectra of the clusters caused by the Brownian diffusion of aggregates on the chamber walls.

The electron-microscopic analysis provided data for estimating the function of size distribution of the deposited particles $n_g(L)$ which was approximated by a gamma distribution with a 10% error. The rate of deposition of clusters with size $L = L_{\max}$ was found from the expression

$$V(L) = \frac{n_g(L)}{n(L)\Delta t}\,, \tag{35}$$

where $n(L)$ is the particle size distribution function in the coagulation chamber averaged over deposition time Δt = 60 min.

The data obtained are shown in Fig. 11a. They seem to indicate that fractal clusters exhibit high resistance to sedimentation, with an anomalous sedimentation rate dependence (in comparison with the Stokes one, curve *4*) for large clusters.

Indeed, these data reflect one of the principal intrinsic features of fractal objects, i.e. a decrease in the mean cluster density with growth in compliance with the following rule

$$\rho(R) \sim \rho_0 \left(\frac{r_0}{R}\right)^{3-D}\,, \tag{36}$$

where ρ_0 and r_0 are the density and the size repectively of primary kernels.

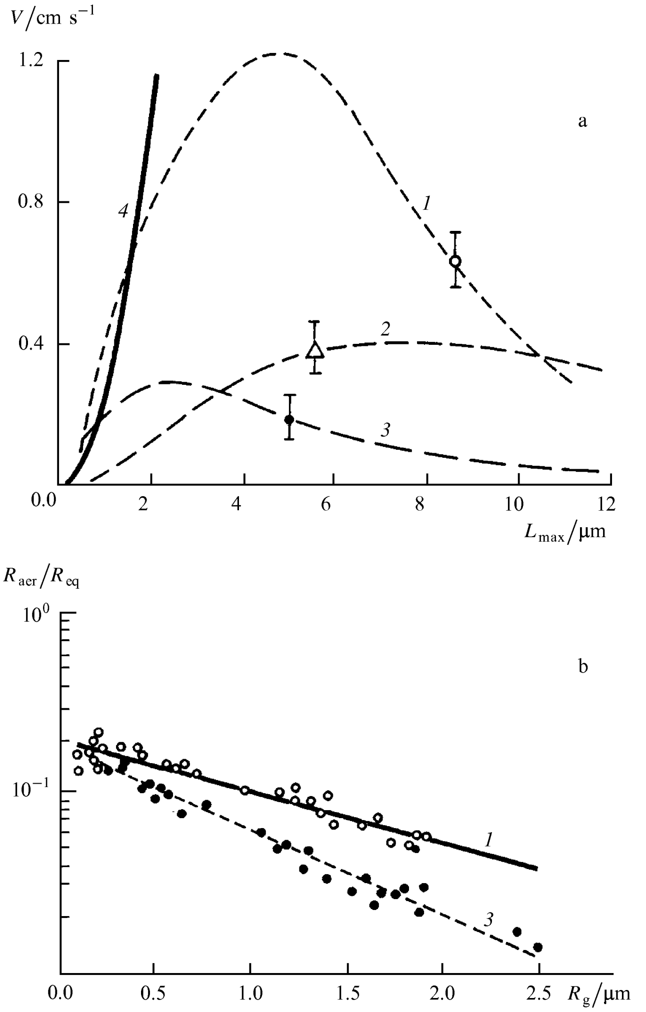

Figure 11. Aerodynamic properties of fractal clusters: (a) gravitational sedimentation rate v in relation to linear size $L_{\max}$ (curve *4* is calculated from the Stokes formula [33]), (b) reduced aerodynamic radius $R_{\text{aer}}/R_{\text{eq}}$ in relation to radius of gyration R_g. See Fig. 10 for notations.

A consequence of the low fractal cluster density is the small aerodynamic (Stokes) radius R_{aer} (compared with the equivalent radius $R_{\text{eq}} = N^{1/3} r_0$) [57]. Fig. 11b demonstrates that the difference between R_{aer} and R_{eq} is most pronounced for aggregates formed during cluster–cluster association of modified particles (curve *3*).

Analysis of the aerodynamic behaviour of fractal clusters in gravitational and electric fields constitutes the basis of 'in situ' methods for the assessment of fractal dimension [58] from its relationship with cluster density and standard geometric characteristics.

The relationship between the equivalent and sedimentation radii of a cluster is defined by the expression [59]

$$R_{\text{eq}} = R_s^{2D/3(D-1)}\,. \tag{37}$$

With the aid of this relation and independently determined values of R_{eq} (e.g. by means of weight-computation analysis) and R_s (by sedimentation measurements), it is possible to calculate the fractal dimension of the aggregate.

However, Eqn (37) is valid only in the approximation of the Stokes regime of the cluster in a gaseous medium which cannot be regarded as totally correct. Although the aggregate size as a rule substantially exceeds the length of the free path of a molecule in the gas, the diameter of the initial dispersed particles is comparable with and often significantly smaller than the latter value.

It has been shown [60] that the drag exerted by the medium depends on the dispersion of gas molecules on primary elements of the structure, owing to the structural features of fractal aggregates. The free path of molecules λ_f predicted by this mechanism at the mean particle number density in the cluster

$$n = \frac{(R/r_0)^D}{4\pi R_0^3/3} \tag{38}$$

is estimated from the relation

$$\lambda_f = \frac{1}{\pi r_0^2 n} \approx R\left(\frac{r_0}{R}\right)^{D-2} . \tag{39}$$

According to Eqn (39), condition $\lambda_f > R$ is fulfilled for fractal clusters with $D < 2$. The resulting drag can be considered as the sum of the forces experienced by all particles in the aggregate:

$$F = \frac{32}{3v_T} N r_0^{2-D_R D_v} k_B T = \frac{8}{3} N r_0^{2-D_R D_v} (2\pi m k_B T)^{1/2} , \tag{40}$$

where N is the number density of molecules in the gas and v_T is their mean thermal velocity.

The condition of applicability of Stokes formula for the force opposing the motion of the aggregate has the form

$$\lambda \ll R , \quad \lambda_f \ll R , \tag{41}$$

where λ is the free path length of the molecules prior to their collision with one another. Obviously, condition (41) is not fulfilled for fractal aggregates obtained in gaseous phase which makes both the Stokes formula and Eqn (37) inapplicable to such systems.

This inference is supported by the dependences $v(L_{\max})$ found by experiments, which are strikingly different from the respective curve for Stokes particles (Fig. 11a).

Transport processes in macroscopic aerogel-like structures also involve molecular kinetic mechanisms. In particular, the pressure drop Δp across an aerogel plate through which a gas is flowing at velocity j is found from [60]:

$$j = \frac{3\Delta p}{2 l \rho S \,\bar{\rho} (2 m k_B T/\pi)^{1/2}} , \tag{42}$$

where ρ is the gas density, l is the plate thickness, S and $\bar{\rho}$ are the specific surface and mean density of the material respectively.

Eqn (42) is a variant of the Darcy law for highly porous systems satisfying the conditions

$$\lambda \gg r_0 , \quad l \gg R_c , \tag{43}$$

where R_c is the characteristic size of the region in which the system displays fractal properties.

Aerogels produced by relaxation of aerosol plasma are very sparse structures of thin interlaced threads with diameter comparable to that of the primary kernels from which they arise (10–30 nm). Such structures differ from other fibrous materials in that they have large specific surface and low aerodynamic resistance. Combination of these properties is a prerequisite for gas filtration by which dispersed impurities can be effectively removed.

Table 6. Breakthrough coefficients for NaCl particles.

Type of filter	Δp/mm H_2O	Particle size/μm				
		0.05	0.1	0.2	0.5	1
Carbon aerogel	6	0.04	0.12	0.22	0.17	< 0.02
AFA-VP	6	0.09	0.22	0.30	0.16	< 0.02
Carbon aerogel-coated, AFA-VP filter	8	0.04	0.05	0.07	0.10	< 0.02

The results of an experiment designed to compare the capture of NaCl particles by carbon aerogel and a standard vinyl perchloride aerosol filter (AFA-VP) are listed in Table 6. The uptake was assessed by calculating the breakthrough coefficient — the ratio of the number of particles that pass through the filter to their initial total number. Parameters of the filters were measured at a linear flow velocity of 1.8 cm s^{-1}.

The data in Table 6 indicate that, at an equal resistance to the flow, aerogel filters are more efficient. But the best results were obtained with AFA-VP filters coated with aerogel. The microstructure of the resulting material is depicted in Fig. 12.

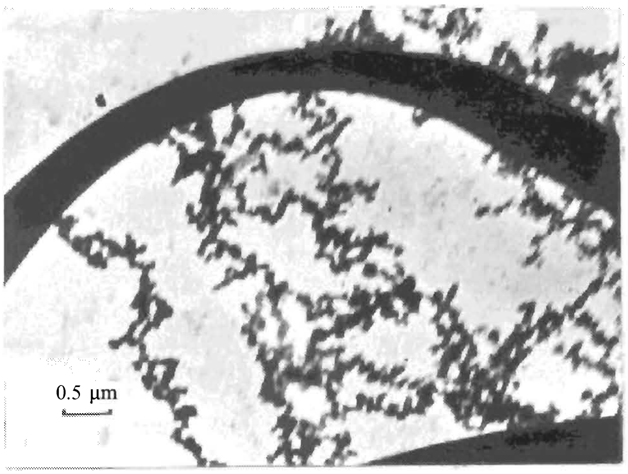

Figure 12. Micrograph of polymeric fibres of the filter modified by filamentary carbon clusters.

The micrograph clearly demonstrates that filamentary carbon structures are responsible for a substantial increase in the surface area of the system and thus contribute to the enhanced trapping, largely by promoting contacts between the particles and the filter and also because of electrostatic attraction [61]. It is emphasised that an average three-fold improvement in capture efficiency (in the size range of 0.1 to 0.5 μm) is associated with only a small rise in resistance to flow.

4.3 Adsorption and capillary condensation on fractal structures

A study of sorption properties including mechanisms of capillary condensation may be of interest if a deeper insight into the structure of fractal objects is to be obtained. However, such investigations of fractal clusters produced in the gaseous phase are not feasible at the level of isolated microscopic structures.

But, since the characteristic size of the adsorbed molecules is significantly smaller than that of cluster-forming primary particles, it seems safe to conclude that structural information about sorption properties of individual clusters will also apply to their bound complexes. Macrosystems of 'frozen' fractal clusters can be regarded as aerogel species which makes them useful in experimentation.

4.3.1 A study of adsorption on fractal structures. Fractal aggregates in the form of a PbI_2 aerogel were obtained and concentrated in an electrodiffusion separator (Fig. 9b). Gauze electrodes with the cell diameter of 70 μm were used in all cascades of the separator.

Cluster growth in the modified separator was reminiscent of the process described in Section 3.1 in that it involved virtually the same aggregation stages. However, the terminal stages of the two processes were different. When the aerodisperse system passed through a gauze electrode, most of the particles were deposited on its surface owing to polarisation interaction and the effect of inertial forces. This resulted in a huge macrocluster in the form of a coating a few millimeters thick which uniformly covered the electrode.

There was a rise in the electric field strength at the tips of filamentary aggregates which enabled new clusters from the gaseous phase to join those previously deposited along the field lines. This eventually led to the formation of a loose large-cell structure (see Fig. 14 below).

It should be emphasised that both primary particles and mature clusters collectively contribute to aerogel growth in this situation, with the latter mechanism assuring faster screening of inner aerogel layers and hence its lower average density. Adjusting the electric field strength provides an effective tool for controlling the relative amount of primary particles in the aerodisperse system and thus of changing the structure of the aerogel [62].

Particles that passed through the first electrode entered the next one where further growth and precipitation occurred, etc. The aerogel thus obtained and removed from the electrode surface was a highly porous substance with bulk density of $0.01-0.03$ g cm^{-3} depending on electric field strength.

The specific surface of PbI_2 aerogel specimens was calculated from nitrogen adsorption values measured by the continuous flow technique with a GHS sorbtograph (Japan), in accordance with the Brunauer–Emmet–Taylor theory [55, 62].

As expected, the effect of the electric field on the growth of the aerogel manifested itself in the formation of looser structures that exhibited an almost linear decrease of fractal dimension with increasing field strength (Fig. 13a). Also, it is worthy of note that very open aerogels had greater specific surface as indicated by the dependence $S(D)$ presented in Fig. 13b.

The plot of S vs D and the results of electron-microscope image analysis (Fig. 14) taken together indicate that changes of the aerogel specific surface were largely due to variation of the mean coordination number υ in the aggregate.

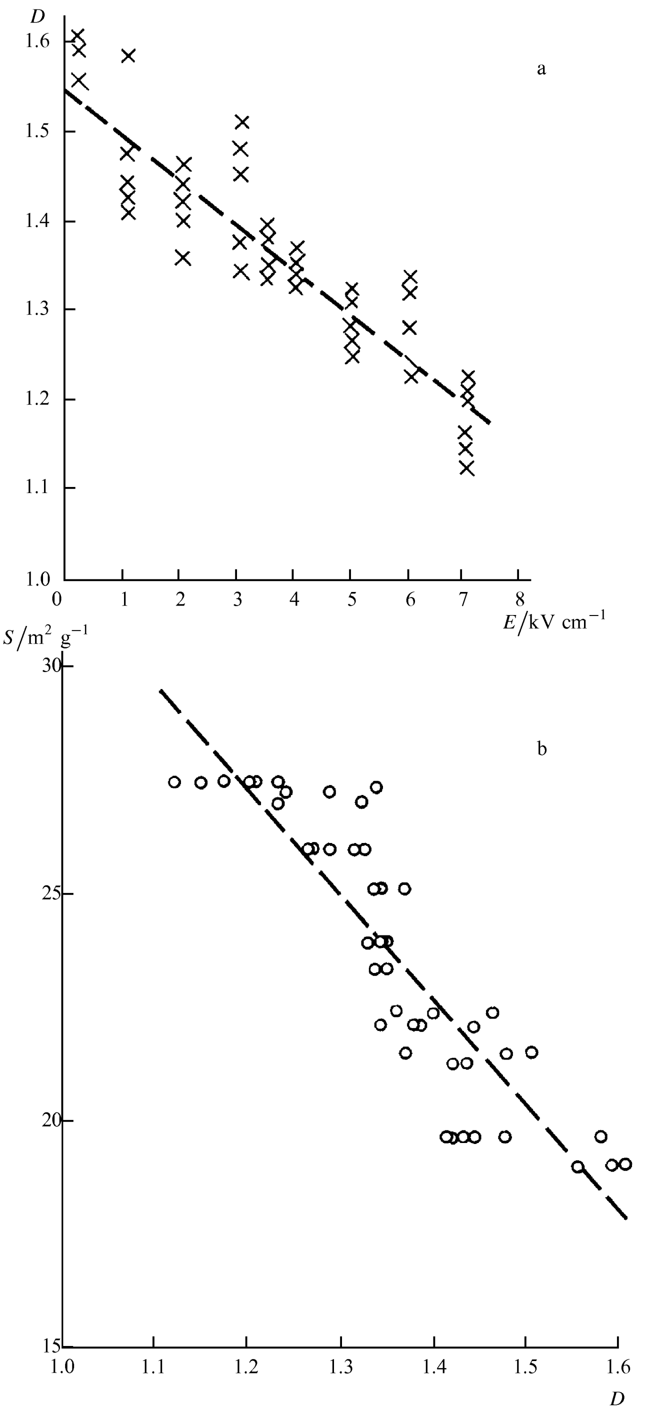

Figure 13. Modification of aerogel structure by the electric field: (a) fractal dimension vs field tension, (b) specific surface vs fractal dimension.

In fact, the specific surface of a system of non-colliding particles is dependent on their total surface area. In the case of smooth monodisperse spheres with radius r_0 and density ρ_0, it is defined by

$$S_0 = \frac{3}{r_0 \rho_0} \,. \tag{44}$$

Aggregation results in a decrease in the adsorption surface of the system by by an amount equal to the sum of the contact surfaces of the particles. Therefore, the approximate expression for the specific surface of an aerogel may be written in the form

$$S = S_0 \left(1 - \frac{S_{\mathrm{cont}}}{S_{\mathrm{part}}} \, \upsilon \right) , \tag{45}$$

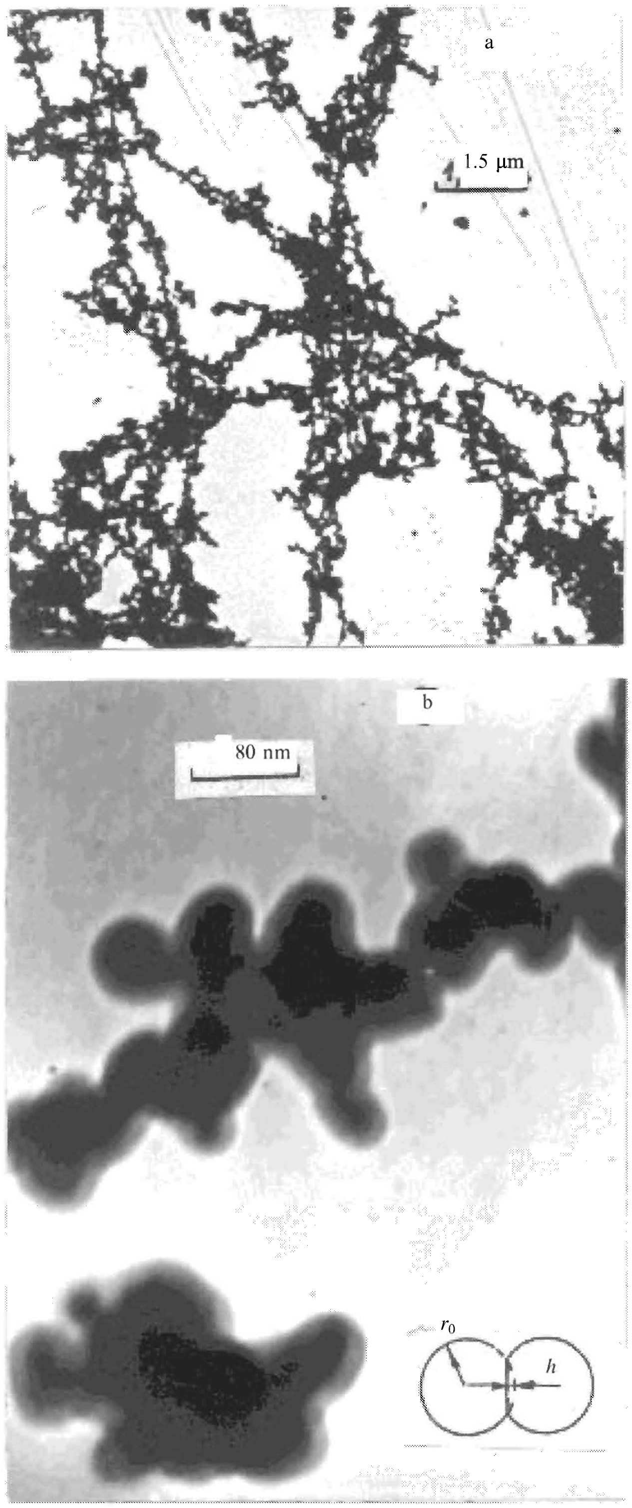

Figure 14. A fragment of aerogel structure obtained in an electric field of 12 kV cm^{-1}; (a) ×10 000, (b) ×260 000.

where S_{part} is the mean surface area of an isolated particle and S_{cont} is the mean surface of a single contact between particles.

In the framework of applicability of formula (45), the relationship between surface area and microstructure of a specimen is totally dependent on the mean coordination number υ which is in turn related to both fractal dimension and radius of gyration by $\upsilon \sim R_{\mathrm{g}}^{2D-d}$ [9].

It has been estimated that the following equality holds in the first approximation for cluster structures having the shape of interconnected loops

$$\upsilon = \eta D \,, \tag{46}$$

where $\eta \to 2$ as the cluster radius $R \to \infty$. Analysis of electron micrographs permits the assessment of this coefficient for real objects. Specifically, for the aerogels investigated in the present study $\eta = 1.8 \pm 0.5$.

Taking into account Eqns (45) and (46) allows the relationship between specific surface and fractal dimension to be written down as

$$S = S_0 \left(1 - \frac{S_{\mathrm{cont}}}{S_{\mathrm{part}}} \eta D \right) \,, \tag{47}$$

Its linear nature is in good agreement with measured values (Fig. 13b).

The best fit to the results obtained with Eqn (47) was when $S_{\mathrm{cont}}/S_{\mathrm{part}} = 0.21$. Similar data for this ratio (0.20 ± 0.08) were obtained by the analysis of electron micrographs (see Fig. 14) with the use of the relationship $S_{\mathrm{cont}}/S_{\mathrm{part}} = h/2r_0$ which implies that the zone of contact has the shape of a spherical segment with height h.

It follows from Fig. 14 and Eqns (46) and (47) that the specific surface of particles not involved in contacts ($\upsilon = 0$) in the present experiment was $S_0 = 53$ m^2 g^{-1} whereas calculations with the use of Eqn (45) for average radius $r_0 = 18$ nm gave $S_0' = 27$ $\mathrm{m}^2\,\mathrm{g}^{-1}$. This discrepancy was most probably the result of neglecting the roughness of the surface. Therefore, the ratio S_0/S_0' which in this case equals 1.95 may be used as a measure of roughness of primary kernels.

To summarise, results of specific surface measurements and morphological analysis of the particles taken together indicate that the main factors which determine the aerogel surface area are the total surface of contacts and the roughness of primary kernels. Roughness is a surface constant and depends on the conditions in which primary particles are generated whereas the total contact surface is a variable depending on the mean coordination number and, ultimately, on the fractal structure of the aerogel.

4.3.2 Capillary condensation. Structure of mesopores. Specific features of capillary condensation were investigated on $\mathrm{Bi_2O_3}$ aerogels [64] obtained as described above, with the exception of the initial stage of generation of primary particles which was modified.

Metallic bismuth was chosen as the starting material to obtain primary particles. Its vapours underwent oxidation to the respective oxide when mixed with a stream of air at 1140 K. Rapid cooling of the final product resulted in its condensation as primary kernels 20 ± 8 nm in size. The resulting aerogel had structural characteristics which depended on the electric field strength in the electrostatic coagulator (modifier).

The specimens thus obtained were used to study capillary condensation by the equilibrium elution technique [65], with benzene as the adsorbent. Functions of pore volume distribution by effective radii were derived from the Kelvin equation [66] and adsorption isotherms.

Characteristic spectra for three different values of fractal dimension D are presented in Fig. 15a. As D decreased, the initial spectrum underwent transformation to a system with multimode pore distribution patterns, with

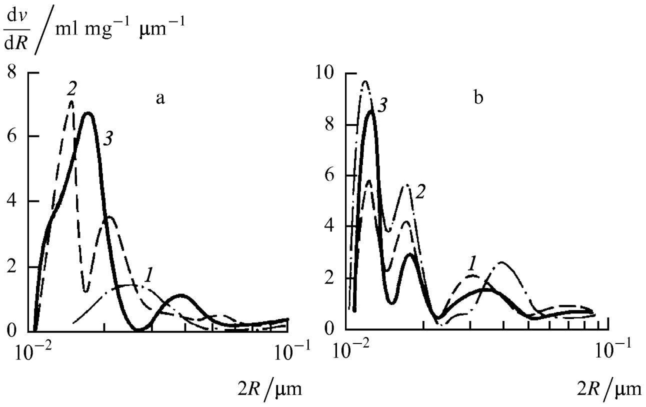

Figure 15. Pore volume distribution by effective radii: (a) at mean fractal dimensions D of 1.60 (*1*), 1.57 (*2*), 1.50 (*3*); (b) at a pressure (kPa) of 0.013 (*1*), 12.6 (*2*), 122.6 (*3*).

a concurrent increase in the intermode space. Analyses of spectra and microphotographs collectively indicate that these changes are related to changes in the fractal structure of the aerogel.

Indeed, primary clusters in the modifier were formed from structural elements of different length which depended on the field strength. The proportion of primary filamentous structures to the size spectrum increased with increasing field strength. For this reason, the pore spectrum of a macroaggregate of such elements was shifted towards larger sizes while the mode number gradually diminished (Fig. 15a, curve *3*).

We tried to produce a controlled shift of the pore spectrum towards smaller sizes in an experiment involving deformation of the aerogel structure. Possible mechanisms responsible for the enhanced density of the fractal aggregate structure have been discussed in Ref. [67].

It should be emphasised that restructuring is a lengthy process with characteristic time varying in the range of 1 hour to a few days. In order to accelerate the process and make it amenable to control, a specimen was first compressed by centrifugation at an appropriate angular velocity for 5 min. Characteristic pore spectra of aerogel specimens obtained by this method are shown in Fig. 15b.

The effect of compression on pores of different size appeared to differ. It was most conspicuous for pores of size 8 nm or more. In this case, the relative proportion of such pores first increased with increasing pressure (curve *2*) which could be accounted for by the destruction of bigger and therefore less stable pores.

The process was reversible, and further increase of compression resulted in the dependence described by curve *3*. Such spectrum restructuring was due to deformation of primary kernels. The effect was most apparent for bigger pores (>8 nm) and less prominent in the case of smaller pores ($\leqslant$5 nm) composed of two or three particles.

To conclude, these experiments demonstrated that fractal structures of weakly-bound nanometer particles formed in the gaseous phase are responsive to modification by external fields. Experimental data on the adsorption patterns in the capillary condensation range may be used to estimate changes in the porosity of the object.

The spectrum of pore distribution with respect to effective radii is shifted towards smaller sizes when the material is influenced by external factors. Taken together, the experimental procedures described in this paper create the necessary prerequisites for the controlled adjustment of sorption characteristics of aerodisperse systems.

5. Conclusion

The evolution of a dispersed system when coagulation is the dominant mechanism of its relaxation proceeds through the formation of fractal clusters, self-similar aggregates of a large number of primary particles. These structures may be considered to represent an intermediate state of condensation starting from the dispersed phase. They are very common in nature and they are formed in many physical, chemical, and biological processes.

There is growing interest in mechanisms of fractal structure generation in the gaseous phase. This has been given an additional incentive by recent advances in basic research and experimental modelling of ball lightning. There is every reason to believe that the fractal structure of plasmoids (e.g. generated by an erosion discharge) underlies the unique physical properties of these long-lived energy- consuming entities which account for their resemblance to natural ball lightnings.

Clearly, there are many important unanswered questions with regard to fractal structures including the relationship between the properties and the dimension of these systems. This problem has been extensively investigated in the physics of condensed state on thin films. In the 1970s, it was unequivocally shown that dimension is not a topological constant with respect to their properties. On the contrary, an object may acquire the properties of a two-dimensional or a three-dimensional system under different conditions. Studies along these lines gave rise to a new area of research referred to as 'physics of reduced dimension' which greatly contributed to the understanding of the nature of such systems and provided practical approaches to many current problems that require a deeper insight into the characteristics of different materials.

The concept of dimension – property relationship acquires special significance in the physics of fractal systems because it provides a methodology for future in-depth studies. It is in this context that we intended to present results of our experiments, focusing on the relationship between fractal dimension and aerodynamic or sorption properties of the object.

Further progress in research on fractal aggregates is firmly tied to the solution of a number of technical problems on ways to generate fractal clusters with desired morphological characteristics. It follows from the present review that there can be no universal strategy for achieving this goal. Specific approaches are needed for obtaining specimens, depending on the nature of the starting material and methods of conversion of the material to the condensed phase. For all that, there is little doubt that further technical and methodological progress in experimental studies will yield new data on the physicochemical properties of fractal aggregates. This line of research should be considered as most promising in modern physics.

References

1. Mandelbrot B B *Fractals: Form, Chance and Dimension* (San Francisco: Freeman, 1977)
2. Coleman P H, Pietronero L H *Phys. Rep.* **213** 311 (1992)

3. Meakin P *Phase Transitions and Critical Phenomena* (London: Academic Press, 1988)
4. Vicsek T *Fractal Growth Phenomena* (Singapore: World Scientific, 1989, 1991)
5. Smirnov B M *Fizika Fraktal'nikh Klasterov* (Physics of Fractal Clusters) (Moscow: Nauka, 1991)
6. Berry M V, Percival I C *Opt. Acta* **33** 577 (1986)
7. Peardon A, Anderson R W *J. Am. Phys. Soc.* **48** 5865 (1993)
8. —Colbeck I, Appleby L, Hardman E J *J. Aerosol. Sci.* **21** 327 (1990)
9. Meakin P *Rev. Geophys.* **29** 317 (1991)
10. Wiltzius P *Phys. Rev. Lett.* **58** 710 (1987)
11. Chen Z-Y, Meakin P *Phys. Rev. Lett.* **59** 2121 (1987)
12. Pietronero L, Tosatti E (Eds) *Fractals in Physics* (Amsterdam: North-Holland, 1988)
13. Lushnikov A A et al. *Usp. Fiz. Nauk* **161** (2) 113 (1991) [*Sov. Phys. Usp.* **34** 160 (1991)]
14. Smirnov B M *Usp. Fiz. Nauk* **152** 133 (1987) [*Sov. Phys. Usp.* **30** 420 (1987)]
15. Forrest S R, Witten T A *J. Phys. A* **12** 109 (1979)
16. Lushnikov A A, Pakhomov A V, Chernyaev G A *Dokl. Akad. Nauk SSSR* **292** 86 (1987) [*Sov. Phys. Dokl.* **32** 45 (1987)]
17. Lushnikov A A, Maksimenko V V, Pakhomov A V *J. Aerosol. Sci.* **20** 165 (1989)
18. Matsumoto O, Oonuma H, Uyama H *J. Electrochem. Soc.* **139** L8 (1992)
19. Ugarte D *Chem. Phys. Lett.* **198** 595 (1992)
20. Mikhailov E F, Vlasenko S S *Khim. Fiz.* **9** 1580 (1990)
21. Smirnov B M *Teplofiz. Vys. Temp.* **29** 418 (1991) [*High Temp.* **29** 318 (1991)]
22. Biberman L M, Vorob'ev V S, Yakubov I T *Kinetika Nizkotemperaturnoi Plazmy* (Kinetics of Low-Temperature Plasma) (Moscow: Nauka, 1982)
23. Smirnov B M *Teplofiz. Vys. Temp.* **24** 239 (1986) [*High Temp.* **24** 176 (1986)]
24. Efimov A N (Ed.) *Spravochnik po Neorganicheskim Soedineniyam* (Reference Book of Organic Compounds) (Moscow: Khimiya, 1983)
25. Arshinov A A, Musin A K *Dokl. Akad. Nauk SSSR* **118** 461 (1958) [*Sov. Phys. Dokl.* **3** 99 (1958)]
26. Arshinov A A, Musin A K *Dokl. Akad. Nauk SSSR* **120** 747 (1958) [*Sov. Phys. Dokl.* **3** 588 (1959)]
27. Einbinder H *J Chem. Phys.* **26** 948 (1957)
28. Vorontsov-Vel'yaminov P N, Shevkunov S V *Fiz. Plazmy* **4** 1354 (1978) [*Sov. J. Plasma Phys.* **4** 756 (1978)]
29. Shevkunov S V, Vorontsov-Vel'yaminov P N *Khim. Fiz.* **12** 83 (1993)
30. Lukin A Ya, Stepanov A M *Fiz. Goreniya Vzryva* **19** (4) 45 (1983)
31. Brown W D, Ball R C *J. Phys. A* **18** L517 (1985)
32. Meakin P, Family F *Phys. Rev. A* **36** 5498 (1987)
33. Fuchs N A *Mekhanika Aerozolei* (Mechanics of Aerosols) (Moscow: Izd. AN SSSR, 1955)
34. Jullien R, Meakin P *J. Colloid Interface Sci.* **124** 265 (1989)
35. Nittman J, Daccord G, Stanley H, in Ref. [12] p. 266
36. Allain C, Cloitre M, in Ref. [12] p. 395
37. Robioson D J, Earnshow J C *Phys. Rev. A* **46** 2045 (1992)
38. Feder E *Fractals* (Translated into Russian) (Moscow: Mir, 1991)
39. Botet R, Jullien R *J. Phys. (Paris)* **46** 1543 (1985)
40. Leibovitch L S, Toth T *Phys. Lett. A* **141** 386 (1989)
41. Mandelbrot B, in Ref. [12] p. 9
42. Mikhailov E F, Vlasenko S S *Khim. Fiz.* **10** 1017 (1991)
43. Smirnov B M *Problemy Sharovoi Molnii* (Problems of Ball Lightning) (Moscow: Nauka, 1988)
44. Turkevich L A, Sher G, in Ref. [12] p. 310
45. Plischke M, Racz Z, in Ref. [12] p. 301
46. Smirnov B M *Usp. Fiz. Nauk* **149** 177 (1986) [*Sov. Phys. Usp.* **29** 481 (1986)]
47. Voloshchuk V M *Kineticheskaya Teoriya Koagulyatsii* (Kinetic Theory of Coagulation) (Leningrad: Gidrometeoizdat, 1984)
48. Vicsek T, Family F *Phys. Rev. Lett.* **52** 1669 (1984)
49. Ernst M, in Ref. [12] p. 339
50. Jullien R, Botet R, Kolb M *Phys. Rev. Lett.* **51** 1123 (1983)
51. Lushnikov A A, Maksimenko V V *Zh. Exp. Teor. Fiz.* **102** 1571 (1992) [*Sov. Phys. JETP* **75** 848 (1992)]
52. Lushnikov A A, Maksimenko V V *Zh. Exp. Teor. Fiz.* **103** 1010 (1993) [*J. Exp. Theor. Phys.* **76** 497 (1993)]
53. Maksimenko V V, Krikunov V A, Lushnikov A A *Pis'ma Zh. Exp. Teor. Fiz.* **57** 204 (1993) [*JETP Lett.* **57** 212 (1993)]
54. Pfeifer P, Anvir D *Chem. Phys.* **79** 3566 (1983)
55. Pfeifer P, Obert M, Cole M W *Fractals in the Natural Sciences* (Princeton: Princeton University Press, 1989)
56. Schmidt-Ott A *J. Aerosol Sci.* **19** 553 (1988)
57. Mikhailov E F, Vlasenko S S *Khim. Fiz.* **11** 571 (1992)
58. Emets E P, Novoselova A E, Poluektov P P *Usp. Fiz. Nauk* **164** 959 (1994) [*Phys. Usp.* **37** 881 (1994)]
59. Magill J *J Aerosol. Sci.* **21** S165 (1990)
60. Smirnov B M *Physica Scripta* **49** 615 (1994)
61. Hinds W C *Aerosol Technology* (New York: John Wiley and Sons, 1982)
62. Mikhailov E F, Vlasenko S S, Rishkevich T I *Khim. Fiz.* **11** 996 (1992)
63. Brunauer S *The Adsorption of Gases and Vapors* (Princeton, NJ: Princeton University Press, 1943)
64. Mikhailov E F, Vlasenko S S, Rishkevich T I *Khim. Fiz.* **12** 1159 (1993)
65. Kel'tsev N V *Osnovi Adsorbtsionnoi Tekhniki* (Fundamentals of Adsorption Technology) (Moscow: Khimiya, 1984)
66. Green S, Sing H *Adsorption, Specific Surface and Porosity* (Translated into Russian) (Moscow: Mir, 1984)
67. Meakin P, Jullien R *J. Colloid Interface Sci.* **127** 265 (1989)